
Combating the Instability of Mutual Information-based Losses via Regularization

Kwanghee Choi*¹

Siyeong Lee*²

¹Sogang University

²NAVER LABS

Abstract

Notable progress has been made in numerous fields of machine learning based on neural network-driven mutual information (MI) bounds. However, utilizing the conventional MI-based losses is often challenging due to their practical and mathematical limitations. In this work, we first identify the symptoms behind their instability: (1) the neural network not converging even after the loss seemed to converge, and (2) saturating neural network outputs causing the loss to diverge. We mitigate both issues by adding a novel regularization term to the existing losses. We theoretically and experimentally demonstrate that added regularization stabilizes training. Finally, we present a novel benchmark that evaluates MI-based losses on both the MI estimation power and its capability on the downstream tasks, closely following the pre-existing supervised and contrastive learning settings. We evaluate six different MI-based losses and their regularized counterparts on multiple benchmarks to show that our approach is simple yet effective.

2016, Belghazi et al., 2018, van den Oord et al., 2018, Hjelm et al., 2019], where others introduce MI-based methodologies identifying the relationship between input, output, and hidden variables [Tishby and Zaslavsky, 2015, Shwartz-Ziv and Tishby, 2017, Saxe et al., 2018]. Furthermore, recent self-supervised losses use contrastive losses, where its origin can be traced back to MI-based losses [Cheng et al., 2020, Hénaff, 2020, Chuang et al., 2020].

Although many have shown computational tractability and usefulness of MI-based losses, others still struggle with their instability during optimization. Contrastive learning literature with MI-based losses such as Chen et al. [2020], He et al. [2020] use huge batch sizes to reduce the variance of losses. Bardes et al. [2021] adds a regularization term to the neural network embeddings to stabilize the training. McAllester and Stratos [2020] and Song and Ermon [2020] further provide theoretical limitations of variational MI estimators, arguing that the limited batch size induces a MI estimation variance too large to handle. We argue that mitigating the variance of MI-based losses is critical for stabilizing training, where it is well known that more stable optimization of neural networks yields better predictive performance on the downstream tasks [Rothfuss et al., 2019, Bear and Cushman, 2020, Chavdarova et al., 2019, Richter et al., 2020, Zeng et al., 2020, Colombo et al., 2021].

In this paper, we concentrate on identifying the cause behind the instability of MI-based losses and propose a simple yet effective regularization method that can be applied to various MI-based losses. We start by analyzing the behaviors of two MI estimators; the MI Neural Estimator (MINE) loss [Belghazi et al., 2018] and Nguyen-Wainwright-Jordan loss (NWJ) loss [Nguyen et al., 2010]. We identify two distinctive behaviors that induce instability during training, drifting and exploding neural network outputs. Based on these observations, we design two novel dual representations of the KL-divergence called Regularized Donsker-Varadhan representation (ReDV) and Regularized NWJ representation (ReNWJ). We show theoretically and experimentally that adding our regularizer term suppresses two behaviors

1 INTRODUCTION

Identifying a relationship between two variables of interest is one of the key problems in mathematics, statistics, and machine learning [Goodfellow et al., 2014, Ren et al., 2015, He et al., 2016, Vaswani et al., 2017]. One of the fundamental approaches is information theory-based measurement, namely the measure of mutual information (MI). Due to its mathematical soundness and the rise of deep learning, many have designed differentiable MI-based losses for neural networks. Some utilize the MI-based losses to bridge the gap between latent variables and representations in generative adversarial networks [Nowozin et al., 2016, Chen et al.,

*These authors contributed equally to this work.

of drifting and exploding, avoiding instability during training. Finally, we design a novel benchmark that bridges the gap between variational MI estimators and real-world tasks, whereas previous works either do not directly show the MI estimation performance or evaluate only on toy problems. We reformulate both the supervised and the contrastive learning problem [Chen et al., 2020, He et al., 2020, Khosla et al., 2020] as MI estimation problems and show that our regularization yields better performance on both perspectives, downstream task and MI estimation performance.

2 BACKGROUND & RELATED WORKS

Definition of MI The mutual information between two random variables X and Y is defined as

$$\begin{aligned} I(X, Y) &= D_{\text{KL}}(\mathbb{P}_{XY} || \mathbb{P}_X \otimes \mathbb{P}_Y) \\ &= \mathbb{E}_{\mathbb{P}_{XY}} \left(\log \frac{d\mathbb{P}_{XY}}{d\mathbb{P}_X \otimes \mathbb{P}_Y} \right) \end{aligned} \quad (1)$$

where \mathbb{P}_{XY} and $\mathbb{P}_X \otimes \mathbb{P}_Y$ are the joint distribution and the product of the marginal distributions, respectively. D_{KL} is the Kullback-Leibler (KL) divergence. Without loss of generality, we consider \mathbb{P}_{XY} and $\mathbb{P}_X \otimes \mathbb{P}_Y$ as being distributions on a compact domain $\Omega \subset \mathbb{R}^d$.

MI through dual representation of D_{KL} We first introduce two dual representations of D_{KL} , as MI is defined using D_{KL} . The most widely known is the Donsker-Varadhan representation D_{DV} [Donsker and Varadhan, 1975]. For given two distribution \mathbb{P} and \mathbb{Q} on some compact domain $\Omega \subset \mathbb{R}^d$,

$$D_{\text{DV}}(X, Y) := \sup_{T: \Omega \rightarrow \mathbb{R}} \mathbb{E}_{\mathbb{P}}(T) - \log(\mathbb{E}_{\mathbb{Q}}(e^T)), \quad (2)$$

where both the expectations $\mathbb{E}_{\mathbb{P}}(T)$ and $\mathbb{E}_{\mathbb{Q}}(e^T)$ are finite. If we substitute \mathbb{P} and \mathbb{Q} into \mathbb{P}_{XY} and $\mathbb{P}_X \otimes \mathbb{P}_Y$, D_{DV} yields the definition of MI. The optimal $T^* = \log \frac{d\mathbb{P}}{d\mathbb{Q}} + C$, where $C \in \mathbb{R}$ can be any constant.

In contrast to D_{DV} , the Nguyen-Wainwright-Jordan representation D_{NWJ} [Nguyen et al., 2010] is induced by the convex conjugate known as Fenchel’s inequality [Hiriart-Urruty and Lemaréchal, 2004]:

$$D_{\text{NWJ}}(X, Y) := \sup_{T: \Omega \rightarrow \mathbb{R}} \mathbb{E}_{\mathbb{P}}(T) - \mathbb{E}_{\mathbb{Q}}(e^{T-1}) \quad (3)$$

The optimal $T^* = \log \frac{d\mathbb{P}}{d\mathbb{Q}} + 1$ is unique unlike the optimal T^* of D_{DV} due to its self-normalizing property [Belghazi et al., 2018]. However, D_{DV} guarantees tighter lower bounds than D_{NWJ} [Ruderman et al., 2012, Polyanskiy and Wu, 2014]. These two representations provide the theoretical soundness for numerous variational MI bounds.

Variational MI estimation With the increasing success of neural networks, several neural network-driven variational bounds of MI are proposed. They are widely employed, such as contrastive learning [van den Oord et al.,

2018, He et al., 2020, Chen et al., 2020] or generative adversarial training [Belghazi et al., 2018, Nowozin et al., 2016]. Variational bounds of MI commonly focus on estimating T^* via a neural network $T_\theta : \Omega \rightarrow \mathbb{R}$, called the statistics network [Belghazi et al., 2018], which outputs a single real value given the input sample pairs.

I_{MINE} [Belghazi et al., 2018] directly maximize D_{DV} as the objective function by feeding the samples (x, y) of \mathbb{P}_{XY} and $\mathbb{P}_X \otimes \mathbb{P}_Y$ into T_θ :

$$\begin{aligned} I_{\text{MINE}}(X, Y) &:= \\ &\mathbb{E}_{\mathbb{P}_{XY}^{(n)}}(T_\theta(x, y)) - \log(\mathbb{E}_{\mathbb{P}_X^{(n)} \otimes \mathbb{P}_Y^{(n)}}(e^{T_\theta(x, y)})), \end{aligned} \quad (4)$$

where $\mathbb{P}^{(n)}$ is the empirical distribution associated to n i.i.d. samples for given distribution \mathbb{P} . Belghazi et al. [2018] also utilizes moving averages of mini-batches to reduce the MI estimation variance caused by the limited batch size.

I_{InfoNCE} [van den Oord et al., 2018] is also commonly used due to its stability and decent performance:

$$I_{\text{InfoNCE}}(X, Y) = \frac{1}{N} \sum_{i=1}^N \log \frac{e^{T_\theta(x_i, y_i)}}{\frac{1}{N} \sum_j e^{T_\theta(x_i, y_j)}} \quad (5)$$

where the N samples $(x_i, y_i)_{i=1}^N$ are drawn from \mathbb{P}_{XY} , which becomes equivalent to using the Softmax function with the negative log loss. I_{InfoNCE} is also equivalent to I_{MINE} up to a constant, but upper bounded by $\log N$, hence not able to estimate large MI values [van den Oord et al., 2018].

Poole et al. [2019] introduced I_{TUBA} , a unified lower bound, by expanding D_{NWJ} [Barber and Agakov, 2003, Nguyen et al., 2010].

$$\begin{aligned} I_{\text{NWJ}}(X, Y) &:= \\ &\mathbb{E}_{\mathbb{P}_{XY}^{(n)}}(T_\theta(x, y)) - \mathbb{E}_{\mathbb{P}_X^{(n)} \otimes \mathbb{P}_Y^{(n)}}(e^{T_\theta(x, y)-1}), \end{aligned} \quad (6)$$

$$\begin{aligned} I_{\text{TUBA}}(X, Y) &:= \mathbb{E}_{\mathbb{P}_{XY}^{(n)}}(T_\theta(x, y)) \\ &- \mathbb{E}_{\mathbb{P}_Y^{(n)}} \left(\mathbb{E}_{\mathbb{P}_X^{(n)}}(e^{T_\theta(x, y)})/a(y) + \log(a(y)) - 1 \right), \end{aligned} \quad (7)$$

where $a(y)$ is the variational parameter. However, unlike I_{MINE} or I_{InfoNCE} , directly using the exponential term often causes numerical instability. Even if T_θ outputs a moderately sized value, e^{T_θ} can easily exceed the floating-point range.

To avoid this problem, Poole et al. [2019] introduce D_{NWJ} -based lower bound I_{JS} by using a softplus-activated neural network as T_θ ,

$$\begin{aligned} I_{\text{JS}}(X, Y) &:= 1 + \mathbb{E}_{\mathbb{P}_{XY}^{(n)}}(T_\theta(x, y)) \\ &- \mathbb{E}_{\mathbb{P}_Y^{(n)} \otimes \mathbb{P}_X^{(n)}}((e^{T_\theta(x, y)})). \end{aligned} \quad (8)$$

Variance problem of MI estimators Despite the variety of bounds proposed, many still suffer from the bias-variance trade-off [Poole et al., 2019]. McAllester and Stratos [2020] and Song and Ermon [2020] prove that the I_{MINE} estimator must have a batch size proportional to the exponential of true MI to control the variance of the estimation.

Many bounds try to mitigate this problem by reducing the variance of low-biased estimators, such as by interpolating with a low variance bound [Poole et al., 2019] or dropping the formal theoretical guarantees [McAllester and Stratos, 2020]. Song and Ermon [2020] proposed I_{SMILE} to clip the range of T_θ trained with I_{MINE} , sacrificing the estimation quality to reduce the variance.

$$I_{\text{SMILE}}(X, Y) := \mathbb{E}_{\mathbb{P}_{XY}^{(n)}}(T_\theta(x, y)) - \log(\mathbb{E}_{\mathbb{P}_X^{(n)} \otimes \mathbb{P}_Y^{(n)}}(\text{clip}(e^{T_\theta(x, y)}, e^{-\tau}, e^\tau))), \quad (9)$$

where $\text{clip}(v, l, u) = \max(\min(v, u), l)$ for $v, u, l \in \mathbb{R}$.

Practical usages of MI MI-based losses are often applied in generative modeling, such as for better mode coverage [Belghazi et al., 2018] or learning disentangled representations without supervision [Chen et al., 2016, Ojha et al., 2020, Li et al., 2021b, Jeon et al., 2021]. Representation learning employs MI-based losses [Tian et al., 2020b, Hjelm et al., 2019, Tschannen et al., 2020, Cheng et al., 2020, Wu et al., 2020, Wen et al., 2020, Boudiaf et al., 2020, Tian et al., 2020a, Li et al., 2021a] to yield feature extractors that reflect its downstream tasks well. We emphasize that these approaches can be further utilized to measure the performance of MI estimators.

Comparing between MI estimators Toy datasets such as correlated multivariate Gaussian distributions has been widely accepted for the evaluation of MI estimation [Belghazi et al., 2018, Poole et al., 2019, Song and Ermon, 2020, Cheng et al., 2020, Lin et al., 2019]. However, we emphasize that using synthetic data as a definitive benchmark will end up in a disparity with real-world tasks. There have been some approaches that compared different MI estimators on generative modeling [Belghazi et al., 2018, Hjelm et al., 2019] or representational learning [Tian et al., 2020b]. However, finding the ideal MI for each downstream task is not trivial, making it impossible to directly assess the MI estimation quality. Moreover, Tschannen et al. [2020] and Tian et al. [2020b] showed the gap between MI estimation quality and downstream performance on specific tasks. Hence, it is crucial to evaluate both perspectives. The closest work to our benchmark is the consistency test of Song and Ermon [2020] using CIFAR-10 [Krizhevsky, 2009] and MNIST [LeCun et al., 1998]. However, the test only offered to assess the ratio of two separate MI estimations, making it difficult to separately measure the quality of each estimation.

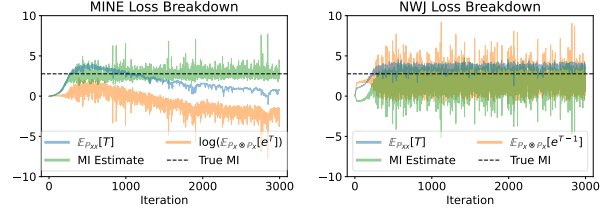


Figure 1: Training T_θ using I_{MINE} and I_{NWJ} with batch size 100 for 3000 iterations. We breakdown the MI loss into two components. We split I_{MINE} into first term $\mathbb{E}_{\mathbb{P}_{XX}}(T)$ and second term $\log \mathbb{E}_{\mathbb{P}_X \otimes \mathbb{P}_X}(e^T)$. Similarly, we split I_{NWJ} into first term $\mathbb{E}_{\mathbb{P}_{XX}}(T)$ and second term $\mathbb{E}_{\mathbb{P}_X \otimes \mathbb{P}_X}(e^{T-1})$.

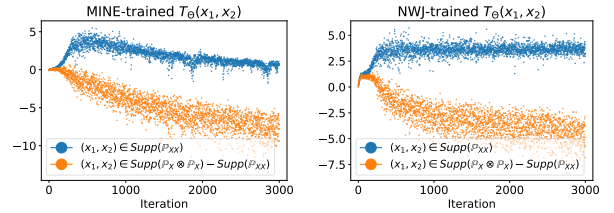


Figure 2: Training T_θ using I_{MINE} and I_{NWJ} with batch size 100 for 3000 iterations. We observe the statistics network outputs $T_\theta(x_1, x_2)$, where we split the outputs into two: $(x_1, x_2) \in \text{Supp}(\mathbb{P}_{XX})$ and $(x'_1, x'_2) \in \text{Supp}(\mathbb{P}_X \otimes \mathbb{P}_X) \setminus \text{Supp}(\mathbb{P}_{XX})$.

3 INSTABILITY OF MI BOUNDS

To demonstrate and analyze the instability of variational MI bounds, we design a synthetic problem with the One-hot dataset. We then solve the task via I_{MINE} and I_{NWJ} , which are the losses derived from the two most commonly used representations of KL-divergence, D_{DV} and D_{NWJ} , respectively. Both losses consist of two terms, each derived from the statistics of joint distribution $\mathbb{E}_{\mathbb{P}_{XY}}$ and the product of marginal distributions $\mathbb{E}_{\mathbb{P}_X \otimes \mathbb{P}_Y}$. Hence, to observe the behavior of each loss during training, we plot the two terms separately. Also, to observe how each distribution differ by the statistics network outputs $T_\theta(x, y)$, we plot each output from $(x, y) \sim \text{Supp}(\mathbb{P}_{XY})$ and $(x, y) \sim \text{Supp}(\mathbb{P}_X \otimes \mathbb{P}_Y) \setminus \text{Supp}(\mathbb{P}_{XY})$, where we denote the support of \mathbb{P} as $\text{Supp}(\mathbb{P})$. Support is the set of values that the random variable can take [Taboga, 2021].

One-hot Dataset We design a one-hot discrete problem with uniform distribution $X \sim U(1, N)$ to estimating $I(X, X) = \log N$ for a given integer N . This task is intentionally created to easily discern samples $(x, x) \sim \mathbb{P}_{XX}$ from $(x, x) \sim \mathbb{P}_X \otimes \mathbb{P}_X$, so that we can directly observe its network outputs $T_\theta(x, x)$.

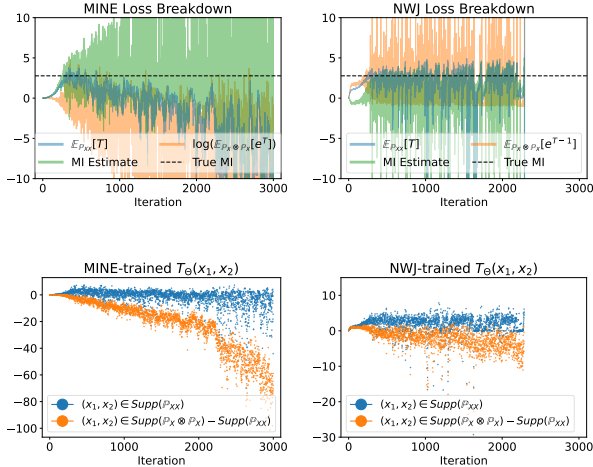


Figure 3: Training T_θ using I_{MINE} and I_{NWJ} with a reduced batch size of 32 for 3000 iterations. MI estimate diverges for both cases. Also, I_{NWJ} incurs exploding T_θ outputs, hence the empty plot after 23k iterations.

Seemingly Stable Case We first observe the behaviors of the statistics network T_θ when the losses are seemingly stable, producing a successful MI estimate. Fig. 1 shows the MI estimates and the two terms that construct each MI estimate per batch. We observe that the first and the second term estimates of I_{MINE} , unlike I_{NWJ} , drifting in parallel even after the MI estimate converge. This is due to the free constant term C in the optimal T^* of D_{DV} , where the self-normalizing D_{NWJ} avoids this problem. This drifting phenomenon implies that T_θ is not stable even after the loss seems to be converged, as shown in Fig. 2. Also, the plot demonstrates how T_θ is trained; it isolates the samples $(x, y) \sim \mathbb{P}_{XY}$ from the samples $(x, y) \sim \mathbb{P}_X \otimes \mathbb{P}_Y$.

Unstable Case We also demonstrate the behaviors of T_θ when the losses get unstable in Fig. 3. We reduce the batch size to make the optimization unstable, where this behavior is often reported in multiple works [van den Oord et al., 2018, He et al., 2020, Chen et al., 2020]. However, even though the losses seem unstable, T_θ successfully discerns the samples before the outputs explode. We believe that this is because of how T_θ is optimized during training. The statistics network outputs $T_\theta(x_1, x_2)$ of $(x_1, x_2) \in \text{Supp}(\mathbb{P}_{XX})$ gets increased by the first term but occasionally decreased by the second term. However, $T_\theta(x'_1, x'_2)$ of $(x'_1, x'_2) \in \text{Supp}(\mathbb{P}_X \otimes \mathbb{P}_Y) \setminus \text{Supp}(\mathbb{P}_{XX})$ gets decreased whatsoever, as (x'_1, x'_2) is used only for the second term. This makes the second term more unstable and motivates us to regularize it for better numerical stability during optimization.

To summarize, we suspect the instability of variational bounds comes from two reasons. Firstly, the statistics net-

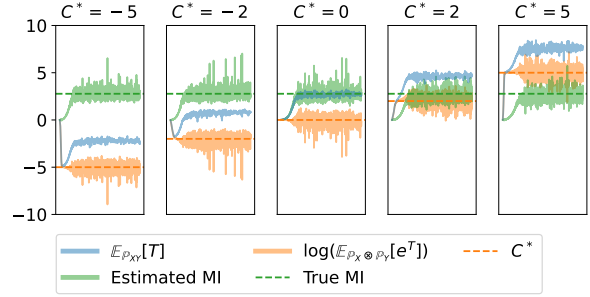


Figure 4: Training T_θ with batch size 100 for 1500 iterations using I_{ReMINE} with different C^* (orange dotted line).

work did not converge even after the loss seemingly converged. We argue that this is due to the unnormalized constant term in the optimal T^* of D_{DV} , where D_{NWJ} successfully avoids via self-normalization. Secondly, the loss gets unstable as $T_\theta(x'_1, x'_2)$ endlessly decrease due to the second term. This observation is also consistent with the theoretical findings of Song and Ermon [2020], McAllester and Stratos [2020], where they show that large variance of the second term leads to failed MI estimation. We claim that the outputs have to be regularized in some form to avoid the instability.

4 STABILIZING THE MI BOUNDS

In this section, we introduce two novel regularized representations and its corresponding losses to tackle the instability during optimization. We show both theoretically and experimentally that adding regularization mitigates the unstable behavior of the statistics network T_θ . We also describe a simple windowing method that can sidestep the batch size limitation problem of the MI estimation problem. We defer all the proofs to the Appendix.

Regularized representations We stabilize the two existing representations D_{DV} and D_{NWJ} by regularizing the second term. We introduce two novel representations: Regularized DV (D_{ReDV}) and Regularized NWJ (D_{ReNWJ}),

$$D_{\text{ReDV}}(X, Y) := \sup_{T: \Omega \rightarrow \mathbb{R}} \mathbb{E}_{\mathbb{P}}(T) - \log(\mathbb{E}_{\mathbb{Q}}(e^T)) - d(\log(\mathbb{E}_{\mathbb{Q}}(e^T)), C^*), \quad (10)$$

$$D_{\text{ReNWJ}}(X, Y) := \sup_{T: \Omega \rightarrow \mathbb{R}} \mathbb{E}_{\mathbb{P}}(T) - \mathbb{E}_{\mathbb{Q}}(e^{T-1}) - d(\mathbb{E}_{\mathbb{Q}}(e^{T-1}), 1), \quad (11)$$

where $C^* \in \mathbb{R}$ is any constant and $d(*, *)$ is a distance function on \mathbb{R} .

Theorem 1. D_{ReDV} and D_{ReNWJ} is a dual representation for D_{KL} such that

$$D_{\text{KL}}(\mathbb{P}||\mathbb{Q}) = D_{\text{ReDV}}(X, Y), \quad (12)$$

$$D_{\text{KL}}(\mathbb{P}||\mathbb{Q}) = D_{\text{ReNWJ}}(X, Y). \quad (13)$$

We emphasize that both representations are not MI-specific but dual representations of D_{KL} , which can be easily extended to numerous variational MI bounds based on D_{DV} and D_{NWJ} . Especially, the newly added regularizer grants D_{ReDV} the normalizing property, effectively solving the drifting problem of D_{DV} .

Regularizing I_{MINE} and I_{NWJ} Based on D_{ReDV} and D_{ReNWJ} , we propose a novel neural network-driven variational MI bound I_{ReMINE} and I_{ReNWJ} by choosing the Euclidean distance $d(x, y) = (x - y)^2$ and the log-Euclidean distance $d(x, y) = (\log x - \log y)^2$, respectively.

$$\begin{aligned}
 I_{\text{ReMINE}}(X, Y) &:= \mathbb{E}_{\mathbb{P}_{XY}^{(n)}}(T_\theta(x, y)) \\
 &\quad - \log(\mathbb{E}_{\mathbb{P}_X^{(n)} \otimes \mathbb{P}_Y^{(n)}}(e^{T_\theta(x, y)})) \\
 &\quad - \lambda(\log(\mathbb{E}_{\mathbb{P}_X^{(n)} \otimes \mathbb{P}_Y^{(n)}}(e^{T_\theta(x, y)})) - C^*)^2,
 \end{aligned} \tag{14}$$

$$\begin{aligned}
 I_{\text{ReNWJ}}(X, Y) &:= \mathbb{E}_{\mathbb{P}_{XY}^{(n)}}(T_\theta(x, y)) \\
 &\quad - \mathbb{E}_{\mathbb{P}_X^{(n)} \otimes \mathbb{P}_Y^{(n)}}(e^{T_\theta(x, y) - 1}) \\
 &\quad - \lambda(\log(\mathbb{E}_{\mathbb{P}_X^{(n)} \otimes \mathbb{P}_Y^{(n)}}(e^{T_\theta(x, y) - 1})))^2,
 \end{aligned} \tag{15}$$

where $C^* \in \mathbb{R}$ is any constant and λ is a hyperparameter that controls the degree of regularization. We can also easily regularize other losses such as I_{InfoNCE} , I_{SMILE} , I_{TUBA} , and I_{JS} in a plug-and-play manner. See Table 1 for more details on its regularized counterparts.

Solving the drifting problem Due to the self-regularizing nature of D_{NWJ} , we must fix $C^* = 1$ for I_{ReNWJ} . We also set $C^* = 0$ for I_{ReMINE} on future experiments, but to demonstrate the ability of the regularizer term to stop the drifting, we experiment with various C^* in Fig. 4. Comparing to I_{MINE} in Fig. 1, we can observe that I_{ReMINE} successfully solves the drifting problem by regularizing the second term to have a single value.

Solving the explosion problem We previously observed the instability of I_{MINE} and I_{NWJ} when using a small batch in Fig. 3. We apply the same setting to I_{ReMINE} and I_{ReNWJ} to observe if the regularizer mitigates the instability problem. Both regularized losses successfully avoid the explosion problem and limit the statistics network outputs $T_\theta(x_1, x_2)$ within a certain boundary. As discussed in Section 3, the second term was the culprit of the variance in MI estimation. The newly added term directly regularizes it to stabilize training, giving the statistics network T_θ additional hints for the second term to converge to a specific value C^* successfully. Furthermore, we empirically found that our regularization works well with I_{SMILE} 's strategy of clipping T_θ . Gradient zeros out for the original I_{SMILE} if $T_\theta(x, y)$ exceeds a certain threshold. This behavior makes T_θ act as if it were frozen, failing to further optimize during training. However, with the regularizer term, we can clip $T_\theta(x, y)$

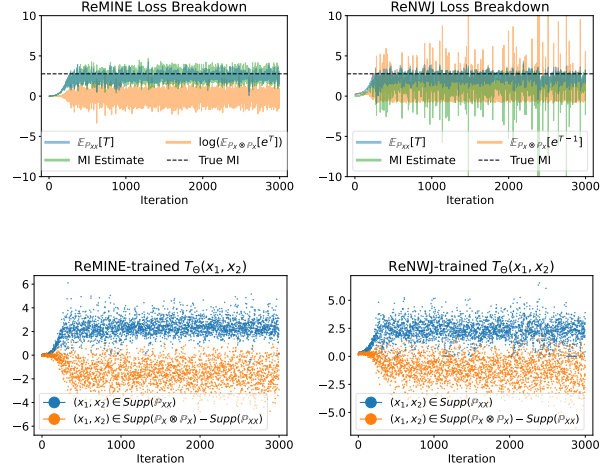


Figure 5: Training T_θ using the regularized counterparts, I_{ReMINE} and I_{ReNWJ} , with the same small batch settings from Fig. 3. Regularization effectively mitigates both instability symptoms, shifting and exploding.

only on first and second term, i.e., on the original loss. Now, clipping filters out the noisy gradients while the gradients calculated from the regularizer avoid freezing T_θ entirely.

Mathematical properties of I_{ReMINE} and I_{ReNWJ} Following Belghazi et al. [2018], we show the soundness of I_{ReMINE} and I_{ReNWJ} in two perspectives, strong consistency and sample complexity. These properties relate to whether the trained T_θ can be sufficiently similar to the optimal T^* .

Theorem 2. I_{ReMINE} and I_{ReNWJ} are strongly consistent.

For the two losses, we also provide the mathematical bound on the number of samples required for the empirical MI estimation at a given accuracy and with high confidence. Similar to Belghazi et al. [2018], let T_θ satisfy L -Lipschitz with respect to the parameter θ such that $|\theta| < K$ and d is dimension of the parameter space of T_θ .

Theorem 3. Assume that T_θ is bounded above by M . Let k be the number of sample means. Given any ϵ, δ of the desired accuracy and confidence parameters, we have

$$\mathcal{P}(|I_{\text{ReMINE}}(X; Y) - I(X, Y)| \leq \epsilon) \geq 1 - \delta, \tag{16}$$

whenever the number n of samples satisfies

$$n \geq \frac{d \log(24KL\sqrt{d}/\epsilon) + 2dM + \log(2/\delta)}{\epsilon^2 k / (2M^2)}. \tag{17}$$

Theorem 4. Assume that $1 \leq |T_\theta| < M$ and $d(x, 1) \leq |x - 1|$. Let k be the number of sample means. Given any ϵ, δ of the desired accuracy and confidence parameters, we have

$$\mathcal{P}(|I_{\text{ReNWJ}}(X; Y) - I(X, Y)| \leq \epsilon) \geq 1 - \delta, \tag{18}$$

whenever the number n of samples satisfies

$$n \geq \frac{d \log(24KL\sqrt{d}/\epsilon) + 2dM + \log(2/\delta)}{\epsilon^2 k / (2M^2)}. \quad (19)$$

Drifting may lead to noisy MI estimate We prove that the variance of the second term on the empirical distributions is affected by the constant term C^* .

Theorem 5. *Let $Q^{(n)}$ be the empirical distributions of n i.i.d. samples from \mathbb{Q} . For the optimal $T_1 = \log \frac{dp}{dq} + C_1$ and $T_2 = \log \frac{dp}{dq} + C_2$ where $C_1 \geq C_2$,*

$$\text{Var}_{\mathbb{Q}}(\mathbb{E}_{Q^{(n)}}(e^{T_1})) \geq \text{Var}_{\mathbb{Q}}(\mathbb{E}_{Q^{(n)}}(e^{T_2})) \quad (20)$$

This implies that unregulated C^* may lead to worse MI estimation quality, as the source of the estimate variance are mainly due to the second term.

Increasing the effective sample size for MI estimation

The drifting problem caused by the unnormalized constant term C^* raises more issues when estimating MI. Poole et al. [2019] use a simple macro-averaging technique, i.e., averaging the estimated MI from each batch. We can also consider a slight modification to the technique, where we call it the micro-averaging technique, by saving all the statistics network outputs $T_\theta(x, y)$ for each batch and producing a single estimate based on all the outputs. However, we proved that both averaging techniques yield wrong final estimates for biased estimators like I_{MINE} [Belghazi et al., 2018], I_{SMILE} [Song and Ermon, 2020], I_{CLUB} [Cheng et al., 2020], and I_{InfoNCE} [van den Oord et al., 2018].

Theorem 6. *(Estimation bias caused by drifting) Both macro- and micro-averaging strategies produce a biased MI estimate when the drifting problem occurs.*

To the contrary, self-normalizing or regularized MI estimators have the upper hand in this perspective. By utilizing all the samples from multiple batches, they can effectively sidestep the batch size limitation problem [McAllester and Stratos, 2020, Song and Ermon, 2020].

5 EXPERIMENTS

5.1 MI ESTIMATION VS. DOWNSTREAM TASK PERFORMANCE

Benchmark Design To measure the performance of the MI estimators, one must design the target task to have the ground truth MI. This constraint led previous works to evaluate the estimators only on artificial toy problems [Belghazi et al., 2018, Poole et al., 2019], where its connection to actual problems is fairly limited. We design the two types of MI estimation tasks with de facto image datasets to improve the existing benchmarks to reflect on the real-world tasks. We defer all the proofs to the Appendix.

Theorem 7. *(Supervised learning) Given a dataset $D = (X, Y)$ where X is an sample, Y is the label for X , and $H(Y)$ is the entropy of the label set, $I(X, Y) = H(Y)$.*

Similarly, the true MI between images from the same class is also tractable based on the same assumption.

Theorem 8. *(Contrastive learning) Consider the dataset $D = (X, Y)$. Let X_1 be a sample drawn from the dataset and X_2 be another sample drawn from the subset with the same label Y to X_1 . Then, $I(X_1, X_2) = I(X_1, Y) = I(X_2, Y) = H(Y)$.*

Note that we assume statistical dependence between the image X and label Y from the point of view of information bottleneck [Tishby and Zaslavsky, 2015]. We derive the theorems above based on the assumption, where Y implicitly determines X .

Based on the above theorems, we use the two MI estimation problems as benchmarks that evaluate the performance of estimators. We intentionally design Theorem 7 and Theorem 8 to mimic the existing tasks closely, namely, supervised and contrastive learning. For Theorem 7, we can set the statistics network $T_\theta(X, Y) = f_\theta(X) \cdot o(Y)$ where $f_\theta(X)$ is the logits obtained from feeding the image X to the classification neural networks and $o(Y)$ is the one-hot representation of the label Y . If we use the InfoNCE estimator, this formulation becomes identical to solving the classification problem using negative log loss with the Softmax function, hence the name being the supervised learning benchmark (SLB). Similarly, for Theorem 8, we can set $T_\theta(X_1, X_2) = f_\theta(X_1) \cdot f_\theta(X_2)$ and use the InfoNCE estimator to yield a commonly used contrastive loss [van den Oord et al., 2018, Chen et al., 2020].

Due to the strict assumption of statistical dependence, the theorems above cannot be used on standard datasets like ImageNet dataset [Deng et al., 2009], as its samples often violate the single-label assumption. However, we can still empirically compare the MI estimators by the relative size of their final MI estimation. We conduct a demo experiment on ImageNet in the Appendix.

Evaluation To verify the performance of MI estimators, we perform our benchmark tasks on the CIFAR10 and CIFAR100 dataset [Krizhevsky, 2009]. As both CIFAR10 and CIFAR100 have a uniform label distribution, ideal MI is $\log 10$ and $\log 100$, respectively. In addition, to check whether this MI estimate task is actually helpful for downstream tasks, we evaluate each estimator on both dimensions: MI estimation and test set accuracy. Similar to the existing settings in the contrastive learning literature [Chen et al., 2020, He et al., 2020], we design the test accuracy of CLB by defining the label estimate \hat{y} of each test set sample x_{Test} to be the label of $x = \text{argmax}_{x \in X_{\text{Train}}} f(x) \cdot f(x_{\text{Test}})$ of the train dataset X_{Train} . Similarly for SLB, we chose

Loss	Loss settings	Regularizer settings
I_{MINE}	No gradient moving average	Euclidean distance
I_{SMILE}	Clipping ($\tau = 10$)	Euclidean distance
I_{InfoNCE}	-	Euclidean distance
I_{NWJ}	-	Log-Euclidean distance, Clipping ($\tau = 10$)
I_{TUBA}	$a(y) = 1$	Log-Euclidean distance, Clipping ($\tau = 10$)
I_{JS}	Estimate with I_{NWJ}	Euclidean distance

Table 1: List of MI estimators with its hyperparameters

$\hat{y} = \operatorname{argmax}_y f(x_{\text{Test}}) \cdot o(y)$ where $o(y)$ is the one-hot encoding of y . We ran the same experiment 5 times with different seeds to yield a 95% confidence interval.

5.2 COMPARISON WITH OUR BENCHMARK

To demonstrate the effectiveness of our novel regularization term, we regularize the two representations, D_{DV} and D_{NWJ} . We test three realizations for each representation, I_{MINE} [Belghazi et al., 2018], I_{SMILE} [Song and Ermon, 2020], and I_{InfoNCE} [van den Oord et al., 2018] for D_{DV} , I_{NWJ} [Nguyen et al., 2010], I_{TUBA} [Poole et al., 2019], and I_{JS} [Hjelm et al., 2019] for D_{NWJ} . We compare the original losses with its regularized counterparts, a total of $6 \times 2 = 12$. We do not apply averaging scheme on any of the losses, and choose the regularization weight $\lambda \in \{0.1, 0.01, 0.001\}$ that shows the best MI estimation results. See Table 1 for more details.

We observe in Table 2 that additional regularization generally induces better performance on both the MI estimation task and the downstream task (test accuracy). Hence, adding the regularizer to a pre-existing supervised or contrastive learning loss seems to be a viable option to increase the performance further. Even when the performance of the regularized loss slightly degrades, its negative impact is minimal. This implies that even for the case where the regularizer is not greatly helpful, it does not greatly hinder optimization. Especially, it is intriguing that many losses, I_{MINE} , I_{ReMINE} , and I_{ReTUBA} , are better than I_{InfoNCE} in SLB, which is used as the de facto standard in classification. Also, I_{SMILE} , I_{NWJ} , and I_{TUBA} fail to converge in CLB, where simply adding a regularization term solves the issue altogether, yielding a competitive or even better performance than all the other losses. Given the fact that numerous contrastive learning literature suffers from instability [Caron et al., 2021, Bardes et al., 2021, Chen et al., 2020, He et al., 2020, Bardes et al., 2021], we emphasize that adding our regularization term can be a simple yet effective method to stabilize training.

Additionally, to observe the impact of regularization strength λ , we plot the benchmark performance for each λ in Fig. 6. We compare the losses on CLB as experimental results suggest that CLB is a more difficult task than SLB, showing significant performance differences between various losses. On CIFAR-10, λ acts as a trade-off parameter

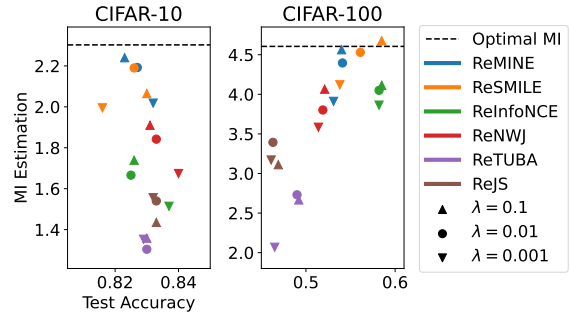


Figure 6: Ablation study on different λ s with CLB CIFAR-10 and CIFAR-100.

between test accuracy and MI estimation quality. Performance trade-off has also been reported in other literature, where better MI estimation does not necessarily deliver better downstream performance [Tschannen et al., 2020, Tian et al., 2020b]. However, compared to CIFAR-100, test accuracy differences are minimal, where MI differences are apparent. I_{ReMINE} and I_{ReSMILE} show excellent MI estimation quality in CIFAR-10 compared to other losses. In contrast, test accuracy and MI estimation quality align well in the CIFAR-100 case. I_{ReSMILE} shows good overall performance, albeit its sensitivity towards regularization strength. $I_{\text{ReInfoNCE}}$, on the other hand, shows stable performance in the downstream task, sacrificing the MI estimation quality. This result is further supported by the prominence of I_{InfoNCE} in the contrastive learning domain. It is yet unclear where the difference between CIFAR-10 and CIFAR-100 comes from, whether it is due to the difference in the level of difficulty of the dataset or the batch size used throughout the training. We leave further analysis as future work.

5.3 COMPARISON WITH THE STANDARD TOY PROBLEM

We provide the quality of MI-based losses on the 20D Correlated Gaussian task [Belghazi et al., 2018, Poole et al., 2019] where the true MI is increased 5 times during optimization in Fig. 7. This experiment demonstrates how stable the MI-based losses estimate MI in a dynamically changing environment. We apply the same settings from

Task		Loss	MI Estimation		Test Accuracy	
			Original	Regularized	Original	Regularized
Supervised Learning Benchmark	CIFAR-10	MINE	2.300 ± 0.003	2.298 ± 0.005	0.850 ± 0.009	0.856 ± 0.004
		SMILE	2.297 ± 0.009	2.300 ± 0.003	0.854 ± 0.008	0.853 ± 0.009
		InfoNCE	2.301 ± 0.002	2.302 ± 0.001	0.845 ± 0.006	0.845 ± 0.005
		NWJ	2.297 ± 0.009	2.294 ± 0.013	0.859 ± 0.003	0.862 ± 0.004
		TUBA	2.297 ± 0.008	2.300 ± 0.003	0.862 ± 0.008	0.859 ± 0.003
		JS	1.944 ± 0.039	2.000 ± 0.049	0.838 ± 0.012	0.842 ± 0.004
	CIFAR-100	MINE	4.597 ± 0.011	4.603 ± 0.001	0.610 ± 0.007	0.610 ± 0.006
		SMILE	4.595 ± 0.015	4.602 ± 0.002	0.601 ± 0.015	0.606 ± 0.007
		InfoNCE	4.594 ± 0.017	4.599 ± 0.005	0.589 ± 0.010	0.593 ± 0.005
		NWJ	4.572 ± 0.055	4.586 ± 0.034	0.558 ± 0.042	0.599 ± 0.009
		TUBA	4.495 ± 0.207	4.603 ± 0.002	0.543 ± 0.055	0.611 ± 0.007
		JS	4.088 ± 0.430	4.240 ± 0.116	0.591 ± 0.026	0.598 ± 0.010
Contrastive Learning Benchmark	CIFAR-10	MINE	2.233 ± 0.674	2.240 ± 0.657	0.812 ± 0.026	0.823 ± 0.012
		SMILE	0.000 ± 0.000	2.065 ± 0.842	0.100 ± 0.001	0.830 ± 0.008
		InfoNCE	1.705 ± 0.462	1.739 ± 0.431	0.830 ± 0.008	0.826 ± 0.006
		NWJ	0.000 ± 0.000	1.910 ± 0.662	0.100 ± 0.000	0.831 ± 0.005
		TUBA	0.000 ± 0.000	1.358 ± 0.590	0.100 ± 0.000	0.830 ± 0.009
		JS	1.552 ± 0.485	1.556 ± 0.546	0.837 ± 0.003	0.832 ± 0.009
	CIFAR-100	MINE	4.634 ± 0.186	4.563 ± 0.162	0.522 ± 0.026	0.540 ± 0.020
		SMILE	0.000 ± 0.000	4.677 ± 0.162	0.012 ± 0.003	0.585 ± 0.007
		InfoNCE	4.112 ± 0.147	4.115 ± 0.145	0.576 ± 0.019	0.585 ± 0.014
		NWJ	0.000 ± 0.000	4.065 ± 0.255	0.010 ± 0.000	0.521 ± 0.025
		TUBA	0.000 ± 0.000	2.731 ± 0.786	0.010 ± 0.000	0.490 ± 0.023
		JS	3.253 ± 0.368	3.393 ± 0.124	0.451 ± 0.020	0.463 ± 0.031

Table 2: Our supervised and contrastive learning benchmark results. We provide the 95% confidence interval of 5 runs for both MI estimation and test accuracy, where we clip the negative MI estimations to 0. We compare the performance of original and regularized loss. **Bold text** and **blue text** indicates the better performance with overlapping and non-overlapping confidence interval, respectively.

Table 1, where we fix the regularization strength $\lambda = 1.0$ for all the losses. With the exception of I_{InfoNCE} , regularized losses show clear superiority over the original losses. Regularization facilitates I_{MINE} and I_{SMILE} to avoid the instability which is mentioned in Section 3. Also, regularization greatly enhances the MI estimation quality of I_{JS} and lessens the variance of both I_{NWJ} and I_{TUBA} .

6 CONCLUSION

In this paper, we identify the two symptoms behind the instability: The statistics network was not converging even after the loss seemed to converge, and its outputs from the product of marginal distribution explode during training. We propose a novel regularization term to mitigate the instability during training by adding to various existing MI-based losses. We theoretically and experimentally demonstrate that the added regularizer directly alleviates the two instability symptoms. Finally, we present a benchmark that evaluates both the MI estimation power and its capability on the downstream tasks by imitating the supervised or contrastive learning settings. We compare six different losses and their regularized

counterparts on various benchmarks to show the method’s effectiveness and broad applicability.

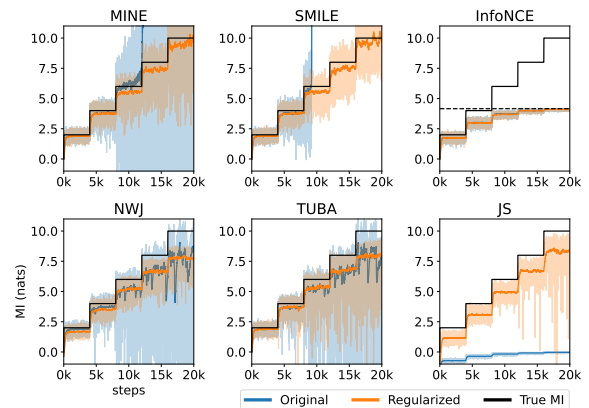


Figure 7: Estimation performance on 20-D Gaussian. The estimated MI (light) and the smoothed estimation with exponential moving average (dark) are plotted for each methods with its regularized counterparts. Black line represents the true MI. Dotted line shows the bound of I_{InfoNCE} due to the limited batch size of 64.

LIMITATIONS AND FUTURE WORKS

We suspect that the instability of MI estimators can also be related to the collapse problem [Bardes et al., 2021, Caron et al., 2021]. Further loss-based approaches to combat this problem by regularizing the network outputs may be helpful. We expect that extending our methods to various contrastive learning losses may yield fruitful results for self-supervised learning, notably for other domains such as text or audio. Also, our mathematical analysis is mainly focused on the drifting problem of I_{MINE} , not the explosion problem of I_{NWJ} . For I_{NWJ} , we suspect that the absence of the log function wrapping the exponential values makes the second term much more susceptible to output explosion due to its numerical instability. The added regularizer gives additional hints for the second term to converge to a specific value. However, we did not expand the discussion further in this paper.

References

- David Barber and Felix V. Agakov. Information maximization in noisy channels : A variational approach. In *Advances in Neural Information Processing Systems 16: Annual Conference on Neural Information Processing Systems NeurIPS*, 2003.
- Adrien Bardes, Jean Ponce, and Yann LeCun. Vicreg: Variance-invariance-covariance regularization for self-supervised learning. *CoRR*, abs/2105.04906, 2021.
- Adam Bear and Fiery Cushman. Loss functions modulate the optimal bias-variance trade-off. In *Proceedings of the 42th Annual Meeting of the Cognitive Science Society - Developing a Mind: Learning in Humans, Animals, and Machines CogSci*, 2020.
- Mohamed Ishmael Belghazi, Aristide Baratin, Sai Rajeswar, Sherjil Ozair, Yoshua Bengio, R. Devon Hjelm, and Aaron C. Courville. Mutual information neural estimation. In *Proceedings of the 35th International Conference on Machine Learning ICML*, 2018.
- Malik Boudiaf, Jérôme Rony, Imtiaz Masud Ziko, Eric Granger, Marco Pedersoli, Pablo Piantanida, and Ismail Ben Ayed. A unifying mutual information view of metric learning: Cross-entropy vs. pairwise losses. In *16th European Conference on Computer Vision ECCV*, 2020.
- Mathilde Caron, Hugo Touvron, Ishan Misra, Hervé Jégou, Julien Mairal, Piotr Bojanowski, and Armand Joulin. Emerging properties in self-supervised vision transformers. In *IEEE/CVF International Conference on Computer Vision ICCV*, 2021.
- Tatjana Chavdarova, Gauthier Gidel, François Fleuret, and Simon Lacoste-Julien. Reducing noise in GAN training with variance reduced extragradient. In *Advances in Neural Information Processing Systems 32: Annual Conference on Neural Information Processing Systems NeurIPS*, 2019.
- Ting Chen, Simon Kornblith, Mohammad Norouzi, and Geoffrey E. Hinton. A simple framework for contrastive learning of visual representations. In *Proceedings of the 37th International Conference on Machine Learning ICML*, 2020.
- Xi Chen, Yan Duan, Rein Houthoofd, John Schulman, Ilya Sutskever, and Pieter Abbeel. Infogan: Interpretable representation learning by information maximizing generative adversarial nets. In *Advances in Neural Information Processing Systems 29: Annual Conference on Neural Information Processing Systems NeurIPS*, 2016.
- Pengyu Cheng, Weituo Hao, Shuyang Dai, Jiachang Liu, Zhe Gan, and Lawrence Carin. CLUB: A contrastive log-ratio upper bound of mutual information. In *Proceedings of the 37th International Conference on Machine Learning ICML*, 2020.
- Ching-Yao Chuang, Joshua Robinson, Yen-Chen Lin, Antonio Torralba, and Stefanie Jegelka. Debaised contrastive learning. In *Advances in Neural Information Processing Systems 33: Annual Conference on Neural Information Processing Systems NeurIPS*, 2020.
- Pierre Colombo, Pablo Piantanida, and Chloé Clavel. A novel estimator of mutual information for learning to disentangle textual representations. In *Proceedings of the 59th Annual Meeting of the Association for Computational Linguistics and the 11th International Joint Conference on Natural Language Processing, ACL/IJCNLP*, 2021.
- Jia Deng, Wei Dong, Richard Socher, Li-Jia Li, Kai Li, and Li Fei-Fei. Imagenet: A large-scale hierarchical image database. In *IEEE Computer Society Conference on Computer Vision and Pattern Recognition CVPR*, 2009.
- Monroe D Donsker and SR Srinivasa Varadhan. Asymptotic evaluation of certain markov process expectations for large time, i. *Communications on Pure and Applied Mathematics*, 28(1):1–47, 1975.
- Ian J. Goodfellow, Jean Pouget-Abadie, Mehdi Mirza, Bing Xu, David Warde-Farley, Sherjil Ozair, Aaron C. Courville, and Yoshua Bengio. Generative adversarial nets. In *Advances in Neural Information Processing Systems 27: Annual Conference on Neural Information Processing Systems NeurIPS*, 2014.
- Kaiming He, Xiangyu Zhang, Shaoqing Ren, and Jian Sun. Deep residual learning for image recognition. In *IEEE Conference on Computer Vision and Pattern Recognition CVPR*, 2016.

- Kaiming He, Haoqi Fan, Yuxin Wu, Saining Xie, and Ross B. Girshick. Momentum contrast for unsupervised visual representation learning. In *IEEE/CVF Conference on Computer Vision and Pattern Recognition CVPR*, 2020.
- Olivier J. Hénaff. Data-efficient image recognition with contrastive predictive coding. In *Proceedings of the 37th International Conference on Machine Learning ICML*, 2020.
- Jean-Baptiste Hiriart-Urruty and Claude Lemaréchal. *Fundamentals of convex analysis*. Springer Science & Business Media, 2004.
- R. Devon Hjelm, Alex Fedorov, Samuel Lavoie-Marchildon, Karan Grewal, Philip Bachman, Adam Trischler, and Yoshua Bengio. Learning deep representations by mutual information estimation and maximization. In *7th International Conference on Learning Representations ICLR*, 2019.
- Insu Jeon, Wonkwang Lee, Myeongjang Pyeon, and Gunhee Kim. Ib-gan: Disentangled representation learning with information bottleneck generative adversarial networks. In *Thirty-Fifth AAAI Conference on Artificial Intelligence AAAI*, 2021.
- Prannay Khosla, Piotr Teterwak, Chen Wang, Aaron Sarna, Yonglong Tian, Phillip Isola, Aaron Maschiot, Ce Liu, and Dilip Krishnan. Supervised contrastive learning. In *Advances in Neural Information Processing Systems 33: Annual Conference on Neural Information Processing Systems NeurIPS*, 2020.
- Alex Krizhevsky. Learning multiple layers of features from tiny images. Master's thesis, Department of Computer Science, University of Toronto, 2009.
- Yann LeCun, Léon Bottou, Yoshua Bengio, and Patrick Haffner. Gradient-based learning applied to document recognition. *Proc. IEEE*, 86(11):2278–2324, 1998.
- Junnan Li, Pan Zhou, Caiming Xiong, and Steven C. H. Hoi. Prototypical contrastive learning of unsupervised representations. In *9th International Conference on Learning Representations ICLR*, 2021a.
- Wei Li, Zhixuan Liang, Julian Neuman, Jinlin Chen, and Xiaohui Cui. Multi-generator GAN learning disconnected manifolds with mutual information. *Knowl. Based Syst.*, 212:106513, 2021b.
- Xiao Lin, Indranil Sur, Samuel A. Nastase, Ajay Divakaran, Uri Hasson, and Mohamed R. Amer. Data-efficient mutual information neural estimator. *CoRR*, abs/1905.03319, 2019.
- David McAllester and Karl Stratos. Formal limitations on the measurement of mutual information. In *The 23rd International Conference on Artificial Intelligence and Statistics AISTATS*, 2020.
- XuanLong Nguyen, Martin J. Wainwright, and Michael I. Jordan. Estimating divergence functionals and the likelihood ratio by convex risk minimization. *IEEE Trans. Inf. Theory*, 56(11):5847–5861, 2010.
- Sebastian Nowozin, Botond Cseke, and Ryota Tomioka. f-gan: Training generative neural samplers using variational divergence minimization. In *Advances in Neural Information Processing Systems 29: Annual Conference on Neural Information Processing Systems NeurIPS*, 2016.
- Utkarsh Ojha, Krishna Kumar Singh, Cho-Jui Hsieh, and Yong Jae Lee. Elastic-infogan: Unsupervised disentangled representation learning in class-imbalanced data. In *Advances in Neural Information Processing Systems 33: Annual Conference on Neural Information Processing Systems NeurIPS*, 2020.
- Yury Polyanskiy and Yihong Wu. Lecture notes on information theory. *Lecture Notes for ECE563 (UIUC)*, 6 (2012-2016):7, 2014.
- Ben Poole, Sherjil Ozair, Aäron van den Oord, Alexander A. Alemi, and George Tucker. On variational bounds of mutual information. In *Proceedings of the 36th International Conference on Machine Learning ICML*, 2019.
- Shaoqing Ren, Kaiming He, Ross B. Girshick, and Jian Sun. Faster R-CNN: towards real-time object detection with region proposal networks. In *Advances in Neural Information Processing Systems 28: Annual Conference on Neural Information Processing Systems NeurIPS*, 2015.
- Lorenz Richter, Ayman Boustati, Nikolas Nüsken, Francisco J. R. Ruiz, and Ömer Deniz Akyildiz. Vargrad: A low-variance gradient estimator for variational inference. In *Advances in Neural Information Processing Systems 33: Annual Conference on Neural Information Processing Systems NeurIPS*, 2020.
- Jonas Rothfuss, Dennis Lee, Ignasi Clavera, Tamim Asfour, and Pieter Abbeel. Promp: Proximal meta-policy search. In *7th International Conference on Learning Representations ICLR*, 2019.
- Avraham Ruderman, Mark D. Reid, Dario García-García, and James Petterson. Tighter variational representations of f-divergences via restriction to probability measures. In *Proceedings of the 29th International Conference on Machine Learning ICML*, 2012.
- Andrew M. Saxe, Yamini Bansal, Joel Dapello, Madhu Advani, Artemy Kolchinsky, Brendan D. Tracey, and David D. Cox. On the information bottleneck theory of deep learning. In *6th International Conference on Learning Representations ICLR*, 2018.
- Ravid Shwartz-Ziv and Naftali Tishby. Opening the black box of deep neural networks via information. *CoRR*, abs/1703.00810, 2017.

Jiaming Song and Stefano Ermon. Understanding the limitations of variational mutual information estimators. In *8th International Conference on Learning Representations ICLR*, 2020.

Marco Taboga. *Support of a random variable*. Kindle Direct Publishing, 2021. URL <https://www.statlect.com/glossary/support-of-a-random-variable>.

Yonglong Tian, Dilip Krishnan, and Phillip Isola. Contrastive multiview coding. In *16th European Conference on Computer Vision ECCV*, 2020a.

Yonglong Tian, Chen Sun, Ben Poole, Dilip Krishnan, Cordelia Schmid, and Phillip Isola. What makes for good views for contrastive learning? In *Advances in Neural Information Processing Systems 33: Annual Conference on Neural Information Processing Systems NeurIPS*, 2020b.

Naftali Tishby and Noga Zaslavsky. Deep learning and the information bottleneck principle. In *IEEE Information Theory Workshop ITW*, 2015.

Michael Tschannen, Josip Djolonga, Paul K. Rubenstein, Sylvain Gelly, and Mario Lucic. On mutual information maximization for representation learning. In *8th International Conference on Learning Representations ICLR*, 2020.

Aäron van den Oord, Yazhe Li, and Oriol Vinyals. Representation learning with contrastive predictive coding. *CoRR*, abs/1807.03748, 2018.

Ashish Vaswani, Noam Shazeer, Niki Parmar, Jakob Uszkoreit, Llion Jones, Aidan N. Gomez, Lukasz Kaiser, and Illia Polosukhin. Attention is all you need. In *Advances in Neural Information Processing Systems 30: Annual Conference on Neural Information Processing Systems NeurIPS*, 2017.

Liangjian Wen, Yiji Zhou, Lirong He, Mingyuan Zhou, and Zenglin Xu. Mutual information gradient estimation for representation learning. In *8th International Conference on Learning Representations ICLR*, 2020.

Mike Wu, Chengxu Zhuang, Milan Mosse, Daniel Yamins, and Noah D. Goodman. On mutual information in contrastive learning for visual representations. *CoRR*, abs/2005.13149, 2020.

Fanyu Zeng, Chen Wang, and Weitian Wang. Visual navigation with asynchronous proximal policy optimization in artificial agents. *J. Robotics*, 2020:8702962:1–8702962:7, 2020.

Combating the Instability of Mutual Information-based Losses via Regularization (Supplementary material)

Kwanghee Choi^{*1}

Siyeong Lee^{*2}

¹Sogang University
²NAVER LABS

A PROOFS

In this section, we provide proof of all theoretical results mentioned in the manuscript.

A.1 PROOF OF THE D_{REDV} REPRESENTATION

In this subsection, we consider two probability distributions \mathbb{P} and \mathbb{Q} , with \mathbb{P} absolutely continuous with respect to \mathbb{Q} . In addition, assume that both distributions are absolutely continuous with respect to Lebesgue measure μ on some compact domain Ω .

We first show that there exists the family of optimal function for the DV representation [Donsker and Varadhan, 1975].

Lemma 9. *All functions of the form $T = \log \frac{d\mathbb{P}}{d\mathbb{Q}} + C^*$ is optimal for the DV representation D_{DV} .*

Proof. To show this theorem, we borrow the proof of the dual representation for the KL divergence [Belghazi et al., 2018].

For a function T , let Δ_T be the gap

$$\Delta_T := D_{\text{KL}}(\mathbb{P}||\mathbb{Q}) - (\mathbb{E}_{\mathbb{P}}(T) - \log \mathbb{E}_{\mathbb{Q}}(e^T)). \quad (21)$$

By Theorem 1 of MINE [Donsker and Varadhan, 1975], we already knew that there exists an optimal function $T^* = \log \frac{d\mathbb{P}}{d\mathbb{Q}} + C$ for some $C \in \mathbb{R}$ such that $\Delta_{T^*} = 0$.

Consider a function $T = \log \frac{d\mathbb{P}}{d\mathbb{Q}} + C^*$ for $C^* \in \mathbb{R}$. The function T can be rewritten as $(T^* - C) + C^*$.

Since

$$\mathbb{E}_{\mathbb{P}}(T) = \mathbb{E}_{\mathbb{P}}(T^* - C + C^*) \quad (22)$$

$$= \mathbb{E}_{\mathbb{P}}(T^*) - C + C^*, \quad (23)$$

and

$$\log(\mathbb{E}_{\mathbb{Q}}(e^T)) = \log(\mathbb{E}_{\mathbb{Q}}(e^{T^* - C + C^*})) \quad (24)$$

$$= \log(e^{C^* - C} \mathbb{E}_{\mathbb{Q}}(e^{T^*})) \quad (25)$$

$$= (C^* - C) + \log(\mathbb{E}_{\mathbb{Q}}(e^{T^*})), \quad (26)$$

$$\mathbb{E}_{\mathbb{P}}(T) - \log(\mathbb{E}_{\mathbb{Q}}(e^T)) = \mathbb{E}_{\mathbb{P}}(T^*) - \log(\mathbb{E}_{\mathbb{Q}}(e^{T^*})). \quad (27)$$

^{*}These authors contributed equally to this work.

Therefore, for the function T ,

$$\Delta_T = D_{KL}(P||Q) - (\mathbb{E}_{\mathbb{P}}(T) - \log \mathbb{E}_{\mathbb{Q}}(e^T)) = D_{KL}(P||Q) - (\mathbb{E}_{\mathbb{P}}(T^*) - \log \mathbb{E}_{\mathbb{Q}}(e^{T^*})) = \Delta_{T^*} = 0. \quad (28)$$

As a result, optimal functions takes the form $T = \log \frac{d\mathbb{P}}{d\mathbb{Q}} + C^*$ for some constant $C^* \in \mathbb{R}$. \square

Theorem. (Theorem 1 restated) Let d be a distance function on \mathbb{R} . For any constant $C^* \in \mathbb{R}$ and any class of functions \mathcal{T} mapping from Ω to \mathbb{R} , we have a novel dual representation of KL divergence

$$D_{ReDV} := \sup_{T \in \mathcal{T}} \mathbb{E}_{\mathbb{P}}(T) - \log(\mathbb{E}_{\mathbb{Q}}(e^T)) - d(\log(\mathbb{E}_{\mathbb{Q}}(e^T)), C^*) = D_{KL}(\mathbb{P}||\mathbb{Q}). \quad (29)$$

Proof. i) For any T ,

$$\mathbb{E}_{\mathbb{P}}(T) - \log(\mathbb{E}_{\mathbb{Q}}(e^T)) - d(\log(\mathbb{E}_{\mathbb{Q}}(e^T)), C^*) \leq \mathbb{E}_{\mathbb{P}}(T) - \log(\mathbb{E}_{\mathbb{Q}}(e^T)). \quad (30)$$

Therefore, $\sup_{T: \Omega \rightarrow \mathbb{R}} \mathbb{E}_{\mathbb{P}}(T) - \log(\mathbb{E}_{\mathbb{Q}}(e^T)) - d(\log(\mathbb{E}_{\mathbb{Q}}(e^T)), C^*) \leq D_{KL}(\mathbb{P}||\mathbb{Q})$.

ii) By the lemma above, there exists $T^* = \log \frac{d\mathbb{P}}{d\mathbb{Q}} + C^*$ such that

$$D_{KL}(\mathbb{P}||\mathbb{Q}) = \mathbb{E}_{\mathbb{P}}(T^*) - \log(\mathbb{E}_{\mathbb{Q}}(e^{T^*})) \quad (31)$$

and

$$\log(\mathbb{E}_{\mathbb{Q}}(e^{T^*})) = \log(\mathbb{E}_{\mathbb{Q}}(e^{C^*} \frac{d\mathbb{P}}{d\mathbb{Q}})) = \log(\int e^{C^*} \frac{d\mathbb{P}}{d\mathbb{Q}} d\mathbb{Q}) = C^*. \quad (32)$$

Therefore,

$$\sup_{T: \Omega \rightarrow \mathbb{R}} \mathbb{E}_{\mathbb{P}}(T) - \log(\mathbb{E}_{\mathbb{Q}}(e^T)) - d(\log(\mathbb{E}_{\mathbb{Q}}(e^T)), C^*) \geq \mathbb{E}_{\mathbb{P}}(T^*) - \log(\mathbb{E}_{\mathbb{Q}}(e^{T^*})) - d(\log(\mathbb{E}_{\mathbb{Q}}(e^{T^*})), C^*) \quad (33)$$

$$= D_{KL}(\mathbb{P}||\mathbb{Q}). \quad (34)$$

Combining i) and ii) finishes the proof. \square

A.2 EXTENSION TO NWJ REPRESENTATION

In this subsection, we show that our regularizer can also be applied to the NWJ representation [Nguyen et al., 2010].

Theorem. Let d be a distance function on \mathbb{R} . We have another dual representation such that

$$D_{ReNWJ} := (\mathbb{P}||\mathbb{Q}) = \sup_{T: \Omega \rightarrow \mathbb{R}} \mathbb{E}_{\mathbb{P}}(T) - \mathbb{E}_{\mathbb{Q}}(e^{T-1}) - d(\mathbb{E}_{\mathbb{Q}}(e^{T-1}), 1) = D_{KL}(\mathbb{P}||\mathbb{Q}). \quad (35)$$

Proof. As d is a distance function, $d(\mathbb{E}_{\mathbb{Q}}(e^{T-1}), 1) \geq 0$.

i) For any T ,

$$\mathbb{E}_{\mathbb{P}}(T) - \mathbb{E}_{\mathbb{Q}}(e^{T-1}) - d(\mathbb{E}_{\mathbb{Q}}(e^{T-1}), 1) \leq \mathbb{E}_{\mathbb{P}}(T) - \mathbb{E}_{\mathbb{Q}}(e^{T-1}). \quad (36)$$

Therefore, $\sup_{T: \Omega \rightarrow \mathbb{R}} \mathbb{E}_{\mathbb{P}}(T) - \mathbb{E}_{\mathbb{Q}}(e^{T-1}) - d(\mathbb{E}_{\mathbb{Q}}(e^{T-1}), 1) \leq D_{KL}(\mathbb{P}||\mathbb{Q})$.

ii) By Poole et al. [2019], there exists $T^* = \log \frac{d\mathbb{P}}{d\mathbb{Q}} + 1$ such that

$$D_{KL}(\mathbb{P}||\mathbb{Q}) = \mathbb{E}_{\mathbb{P}}(T^*) - \mathbb{E}_{\mathbb{Q}}(e^{T^*-1}). \quad (37)$$

$$\mathbb{E}_{\mathbb{P}}(T^*) = \mathbb{E}_{\mathbb{P}}(1 + \log(\frac{d\mathbb{P}}{d\mathbb{Q}})) = 1 + D_{KL}(\mathbb{P}||\mathbb{Q}). \quad (38)$$

and

$$\mathbb{E}_{\mathbb{Q}}(e^{T^*-1}) = \mathbb{E}_{\mathbb{Q}}\left(\frac{d\mathbb{P}}{d\mathbb{Q}}\right) = 1. \quad (39)$$

Therefore,

$$\sup_{T: \Omega \rightarrow \mathbb{R}} \mathbb{E}_{\mathbb{P}}(T) - \mathbb{E}_{\mathbb{Q}}(e^{T-1}) - d(\mathbb{E}_{\mathbb{Q}}(e^{T-1}), 1) \geq \mathbb{E}_{\mathbb{P}}(T^*) - \mathbb{E}_{\mathbb{Q}}(e^{T^*-1}) - d(\mathbb{E}_{\mathbb{Q}}(e^{T^*-1}), 1) \quad (40)$$

$$= D_{KL}(\mathbb{P}||\mathbb{Q}). \quad (41)$$

Combining i) and ii) finishes the proof. \square

A.3 MATHEMATICAL PROPERTIES OF I_{ReMINE}

This subsection presents the proof of the consistency and the sample complexity of I_{ReMINE} . To show these properties, we assume that the input space of the functions below is a compact domain, and all measures are absolutely continuous with respect to the Lebesgue measure. We will restrict to families of feedforward functions with continuous activations, with a single output neuron. To avoid unnecessary heavy notation, we denote $\mathbb{P} = \mathbb{P}_{XY}$ and $\mathbb{Q} = \mathbb{P}_X \otimes \mathbb{P}_Y$ as the joint distribution and the product of marginals unless specified.

First, we define the sample complexity of the MI estimator. As mentioned by Belghazi et al. [2018], this property is related to the *approximation* problem, which addresses the size of the family of function T_{θ} , and the *estimation* problem, which addresses whether it is a reliable estimator.

Definition 1. *The MI estimator $\hat{I}(X, Y)_n$ is strongly consistent if for all $\epsilon > 0$, there exists a positive integer N and a choice of statistics networks such that $\forall n \geq N$, $|I(X, Y) - \hat{I}(X, Y)_n| \leq \epsilon$, where the probability is over a set of samples.*

Consistency proof

Lemma 10. (Approximation) *Let $\eta > 0$. There exists a neural network function T_{θ} with parameters $\theta \in \Theta$ such that*

$$|\hat{I}_{\text{ReMINE}}(X, Y) - I_{\text{ReMINE}}(X, Y)| \leq \eta, \quad (42)$$

where

$$\hat{I}_{\text{ReMINE}}(X, Y) = \sup_{\theta \in \Theta} \mathbb{E}_{\mathbb{P}}(T_{\theta}) - \log(\mathbb{E}_{\mathbb{Q}}(e^{T_{\theta}}) - d(\log(\mathbb{E}_{\mathbb{Q}}(e^{T_{\theta}}), C^*))). \quad (43)$$

Proof. Without loss of generality, we set $T^* = \log \frac{d\mathbb{P}}{d\mathbb{Q}}$. By construction, T^* satisfies:

$$\mathbb{E}_{\mathbb{P}}(T^*) = I(X, Y), \quad \mathbb{E}_{\mathbb{Q}}(e^{T^*}) = 1, \quad \log(\mathbb{E}_{\mathbb{Q}}(e^{T^*})) = 0 \quad (44)$$

For a function T ,

$$I_{\text{ReMINE}}(X, Y) - \hat{I}_{\text{ReMINE}}(X, Y) \quad (45)$$

$$\leq \mathbb{E}_{\mathbb{P}}(T^* - T) + \log(\mathbb{E}_{\mathbb{Q}}(e^T)) + d(\log(\mathbb{E}_{\mathbb{Q}}(e^T), C^*) - d(\log(\mathbb{E}_{\mathbb{Q}}(e^{T^*}), C^*)) \quad (46)$$

$$\leq \mathbb{E}_{\mathbb{P}}(T^* - T) + \log(\mathbb{E}_{\mathbb{Q}}(e^T)) + d(\log(\mathbb{E}_{\mathbb{Q}}(e^T), \log(\mathbb{E}_{\mathbb{Q}}(e^{T^*}))) \quad (47)$$

$$\leq \mathbb{E}_{\mathbb{P}}(T^* - T) + \mathbb{E}_{\mathbb{Q}}(e^T - e^{T^*}) + d(\mathbb{E}_{\mathbb{Q}}(e^T) - 1, 0) \quad (48)$$

where we used the inequality $\log x \leq x - 1$ and $d(\cdot)$ is the distance function induced by norm on \mathbb{R} (e.g., absolute or square error). Fix $\eta > 0$. By the universal approximation theorem, we may choose a feedforward network function $T_{\theta} \leq M$ such that

$$\mathbb{E}_{\mathbb{P}}|T^* - T_{\theta}| \leq \frac{\eta}{3}, \quad \mathbb{E}_{\mathbb{Q}}|T^* - T_{\theta}| \leq \frac{\eta}{3}e^{-M}, \quad \text{and} \quad d(\mathbb{E}_{\mathbb{Q}}|T_{\theta} - T^*|, 0) \leq \frac{\eta}{3 \cdot d(e^M, 0)} \quad (49)$$

Since exp is Lipschitz continuous with constant e^M on $(-\infty, M]$, we have

$$\mathbb{E}_{\mathbb{Q}}|e^{T^*} - e^{T_{\theta}}| \leq e^M \mathbb{E}_{\mathbb{Q}}|T^* - T_{\theta}| \leq \frac{\eta}{3}, \quad (50)$$

and

$$d(\mathbb{E}_{\mathbb{Q}}(e^T) - 1, 0) = d(\mathbb{E}_{\mathbb{Q}}(e^{T_\theta}) - \mathbb{E}_{\mathbb{Q}}(e^{T^*}), 0) = d(\mathbb{E}_{\mathbb{Q}}|e^{T_\theta} - e^{T^*}|, 0) \quad (51)$$

$$\leq d(e^M \mathbb{E}_{\mathbb{Q}}|T_\theta - T^*|, 0) \leq d(e^M, 0) \cdot d(\mathbb{E}_{\mathbb{Q}}|T_\theta - T^*|, 0) \leq \frac{\eta}{3}. \quad (52)$$

From Eq. (48), Eq. (49), Eq. (50), Eq. (51) and the triangular inequality, we then obtain:

$$|\hat{I}_{\text{ReMINE}}(X, Y) - I_{\text{ReMINE}}(X, Y)| < \eta. \quad (53)$$

□

Lemma 11. (Esitimation) Let $\eta > 0$. Given a neural network function T_θ with parameters $\theta \in \Theta$, there exists $N \in \mathbb{N}$ such that

$$\forall n \geq N, \mathcal{P}(|\hat{I}_{\text{ReMINE}}(X, Y)_n - \hat{I}_{\text{ReMINE}}(X, Y)| \leq \eta) = 1, \quad (54)$$

where $\hat{I}_{\text{ReMINE}}(X, Y)_n$ is the ReMINE representation which is empirically obtained by n samples.

Proof. We start by using the triangular inequality to write,

$$\begin{aligned} |\hat{I}_{\text{ReMINE}}(X, Y)_n - \sup_{\theta \in \Theta} \hat{I}_{\text{ReMINE}}(T_\theta)| &\leq \sup_{\theta \in \Theta} |\mathbb{E}_{\mathbb{P}}(T_\theta) - \mathbb{E}_{\mathbb{P}_n}(T_\theta)| + \sup_{\theta \in \Theta} |\log \mathbb{E}_{\mathbb{Q}}(e^{T_\theta}) - \log \mathbb{E}_{\mathbb{Q}_n}(e^{T_\theta})| \\ &\quad + \sup_{\theta \in \Theta} d(|\log \mathbb{E}_{\mathbb{Q}}(e^{T_\theta}) - \log \mathbb{E}_{\mathbb{Q}_n}(e^{T_\theta})|, 0). \end{aligned} \quad (55)$$

Since the function T_θ is uniformly bounded by a constant M and \log is Lipschitz continuous with constant e^M , we have

$$|\log \mathbb{E}_{\mathbb{Q}}(e^{T_\theta}) - \log \mathbb{E}_{\mathbb{Q}_n}(e^{T_\theta})| \leq e^M |\mathbb{E}_{\mathbb{Q}}(e^{T_\theta}) - \mathbb{E}_{\mathbb{Q}_n}(e^{T_\theta})| \quad (56)$$

and

$$d(|\log \mathbb{E}_{\mathbb{Q}}(e^{T_\theta}) - \log \mathbb{E}_{\mathbb{Q}_n}(e^{T_\theta})|, 0) \leq d(e^M, 0) \cdot d(|\mathbb{E}_{\mathbb{Q}}(e^{T_\theta}) - \mathbb{E}_{\mathbb{Q}_n}(e^{T_\theta})|, 0). \quad (57)$$

Since Θ is compact and the feedforward network function is continuous, T_θ and e^{T_θ} satisfy the uniform law of large numbers [Belghazi et al., 2018]. Given $\epsilon > 0$, we can thus choose $N \in \mathbb{N}$ such that $\forall n \geq N$ and with probability 1,

$$\sup_{\theta \in \Theta} |\mathbb{E}_{\mathbb{P}}(T_\theta) - \mathbb{E}_{\mathbb{P}_n}(T_\theta)| \leq \frac{\eta}{3}, \quad (58)$$

$$\sup_{\theta \in \Theta} |\mathbb{E}_{\mathbb{Q}}(e^{T_\theta}) - \mathbb{E}_{\mathbb{Q}_n}(e^{T_\theta})| \leq e^{-M} \frac{\eta}{3}, \quad (59)$$

$$\sup_{\theta \in \Theta} d(|\mathbb{E}_{\mathbb{Q}}(e^{T_\theta}) - \mathbb{E}_{\mathbb{Q}_n}(e^{T_\theta})|, 0) \leq \frac{1}{d(e^M, 0)} \frac{\eta}{3}. \quad (60)$$

Hence, this leads to

$$|\hat{I}_{\text{ReMINE}}(X, Y)_n - \hat{I}_{\text{ReMINE}}(X, Y)| \leq \frac{\eta}{3} + \frac{\eta}{3} + \frac{\eta}{3} = \eta. \quad (61)$$

□

Theorem. ReMINE is strongly consistent.

Proof. Let $\epsilon > 0$. We apply Lemma 10 and Lemma 11 to find a neural network function T_θ and $N \in \mathbb{N}$ such that Eq. (42) and Eq. (54) hold with $\eta = \epsilon/2$. By the triangular inequality, for all $n \geq N$ and with probability one, we have:

$$\begin{aligned} |I(X, Y) - \hat{I}_{\text{ReMINE}}(X, Y)_n| &= |I_{\text{ReMINE}}(X, Y) - \hat{I}_{\text{ReMINE}}(X, Y)_n| \quad (\because \text{Theorem 1}) \\ &\leq |I_{\text{ReMINE}}(X, Y) - \hat{I}_{\text{ReMINE}}(X, Y)| + |\hat{I}_{\text{ReMINE}}(X, Y)_n - \hat{I}_{\text{ReMINE}}(X, Y)| \leq \epsilon \end{aligned} \quad (62)$$

which proves the consistency. □

Sample complexity proof

Theorem. Assume that the function T_θ are M -bounded and \mathcal{L} -lipschitz with respect to the parameter θ . The domain θ is bounded, so that $\|\theta\| \leq K$ for some constant K . When using k mini-batches to estimate MI, we have

$$\mathcal{P}(|\hat{I}_{ReMINE}(X, Y) - I(X, Y)| \leq \epsilon) \geq 1 - \delta \quad (63)$$

whenever the number of samples n for each batch satisfies

$$n \geq \frac{2M^2(d \log(24KL\sqrt{d}/\epsilon) + 2dM + \log(2/\delta))}{\epsilon^2 k}. \quad (64)$$

Proof. As the optimal T^* of I_{ReMINE} is also the solution of I_{MINE} , we can use the same proof process of the Theorem 6 in [Belghazi et al., 2018]. Contrast to MINE [Belghazi et al., 2018], we start from $\mathcal{P}(|\mathbb{E}_{\mathbb{Q}}[f] - \mathbb{E}_{\hat{\mathbb{Q}}}[f]| > \epsilon/6) \leq 2 \exp(-\frac{\epsilon^2 nk}{2M^2})$ by the Hoeffding inequality, because we use $n \cdot k$ samples and our loss function consists of three terms including the regularization term. \square

A.4 MATHEMATICAL PROPERTIES OF I_{ReNWJ}

Consistency Proof We show the proof of the consistency for the ReNWJ based estimator. Same to the proof of ReMINE consistency, we assume that the input space of the functions below is a compact domain, and all measures are absolutely continuous with respect to the Lebesgue measure. We will also restrict to families of feedforward functions with continuous activations, with a single output neuron. We provide a proof for the case where $d(\cdot, \cdot)$ is the log-Euclidean distance in this subsection.

Lemma 12. (Approximation) Let $\eta > 0$. There exists a neural network function T_θ with parameters $\theta \in \Theta$ such that

$$|\hat{I}_{ReNWJ}(X, Y) - I_{ReNWJ}(X, Y)| \leq \eta \quad (65)$$

where

$$\hat{I}_{ReNWJ}(X, Y) = \sup_{\theta \in \Theta} \mathbb{E}_{\mathbb{P}}(T_\theta) - \mathbb{E}_{\mathbb{Q}}(e^{T_\theta-1}) - d(\mathbb{E}_{\mathbb{Q}}(e^{T_\theta-1}), 1). \quad (66)$$

Proof. Without loss of generality, we set $T^* = \log \frac{d\mathbb{P}}{d\mathbb{Q}} + 1$. By construction, T^* satisfies

$$\mathbb{E}_{\mathbb{P}}(T^*) = 1 + I(X, Y), \quad \mathbb{E}_{\mathbb{Q}}(e^{T^*-1}) = 1. \quad (67)$$

For a function T ,

$$I_{ReNWJ}(X, Y) - \hat{I}_{ReNWJ}(X, Y) \quad (68)$$

$$\leq \mathbb{E}_{\mathbb{P}}(T^* - T) + \mathbb{E}_{\mathbb{Q}}(e^{T-1}) - \mathbb{E}_{\mathbb{Q}}(e^{T^*-1}) + d(\mathbb{E}_{\mathbb{Q}}(e^{T-1}), 1) - d(\mathbb{E}_{\mathbb{Q}}(e^{T^*-1}), 1) \quad (69)$$

$$\leq \mathbb{E}_{\mathbb{P}}(T^* - T) + \mathbb{E}_{\mathbb{Q}}(e^{T-1} - e^{T^*-1}) + d(\mathbb{E}_{\mathbb{Q}}(e^{T-1}), \mathbb{E}_{\mathbb{Q}}(e^{T^*-1})) \quad (70)$$

$$\leq \mathbb{E}_{\mathbb{P}}(T^* - T) + e^{-1} \mathbb{E}_{\mathbb{Q}}(e^T - e^{T^*}) + d(\mathbb{E}_{\mathbb{Q}}(e^{T-1}), 1) \quad (71)$$

where $d(\cdot, \cdot)$ is the log-Euclidean distance on \mathbb{R} . Fix $\eta > 0$. By the universal approximation theorem, we may choose a feedforward network function $T_\theta \leq M$ with $M > 1$ such that

$$\mathbb{E}_{\mathbb{P}}|T^* - T_\theta| \leq \frac{\eta}{3}, \quad \mathbb{E}_{\mathbb{Q}}|T^* - T_\theta| \leq \frac{\eta}{3} e^{1-M}, \quad \text{and} \quad d(\mathbb{E}_{\mathbb{Q}}(e^{T_\theta}), e) \leq \frac{\eta}{3}. \quad (72)$$

Since \exp is Lipschitz continuous with constant e^M on $(-\infty, M]$, we have

$$\mathbb{E}_{\mathbb{Q}}|e^{T^*} - e^{T_\theta}| \leq e^M \mathbb{E}_{\mathbb{Q}}|T^* - T_\theta| \leq \frac{\eta}{3} e. \quad (73)$$

And

$$d(\mathbb{E}_{\mathbb{Q}}(e^{T-1}), 1) = d(\mathbb{E}_{\mathbb{Q}}(e^{T_\theta}), \mathbb{E}_{\mathbb{Q}}(e^{T^*})) \leq d(\mathbb{E}_{\mathbb{Q}}(e^{T_\theta}), e) \leq \frac{\eta}{3}. \quad (74)$$

From Eq. (71), Eq. (73), Eq. (74) and the triangular inequality, we then obtain

$$|\hat{I}_{\text{ReNWJ}}(X, Y) - I_{\text{ReNWJ}}(X, Y)| < \eta. \quad (75)$$

□

Lemma 13. (Estimation) *Let $\eta > 0$. Given a neural network function T_θ with parameters $\theta \in \Theta$, there exists $N \in \mathbb{N}$ such that*

$$\forall n \geq N, \mathcal{P}(|\hat{I}_{\text{ReNWJ}}(X, Y)_n - \hat{I}_{\text{ReNWJ}}(X, Y)| \leq \eta) = 1, \quad (76)$$

where $\hat{I}_{\text{ReNWJ}}(X, Y)_n$ is the ReNWJ representation which is empirically obtained by n samples.

Proof. We start by using the triangular inequality to write,

$$\begin{aligned} |\hat{I}_{\text{ReNWJ}}(X, Y)_n - \sup_{\theta \in \Theta} \hat{I}_{\text{ReNWJ}}(T_\theta)| &\leq \sup_{\theta \in \Theta} |\mathbb{E}_{\mathbb{P}}(T_\theta) - \mathbb{E}_{\mathbb{P}_n}(T_\theta)| + \sup_{\theta \in \Theta} |\mathbb{E}_{\mathbb{Q}}(e^{T_\theta-1}) - \mathbb{E}_{\mathbb{Q}_n}(e^{T_\theta-1})| \\ &\quad + \sup_{\theta \in \Theta} d(\mathbb{E}_{\mathbb{Q}}(e^{T_\theta-1}), \mathbb{E}_{\mathbb{Q}_n}(e^{T_\theta-1})). \end{aligned} \quad (77)$$

Since Θ is compact and the feedforward network T_θ is continuous and uniformly bounded by a constant M , T_θ and e^{T_θ} satisfy the uniform law of large numbers [Belghazi et al., 2018]. Given $\epsilon > 0$, we can thus choose $N \in \mathbb{N}$ such that $\forall n \geq N$ and with probability 1,

$$\sup_{\theta \in \Theta} |\mathbb{E}_{\mathbb{P}}(T_\theta) - \mathbb{E}_{\mathbb{P}_n}(T_\theta)| \leq \frac{\eta}{3}, \quad (78)$$

$$\sup_{\theta \in \Theta} e^{-1} |\mathbb{E}_{\mathbb{Q}}(e^{T_\theta}) - \mathbb{E}_{\mathbb{Q}_n}(e^{T_\theta})| \leq \frac{\eta}{3} e^{-M}, \quad (79)$$

$$\sup_{\theta \in \Theta} d\left(\frac{\mathbb{E}_{\mathbb{Q}}(e^{T_\theta})}{\mathbb{E}_{\mathbb{Q}_n}(e^{T_\theta})}, 1\right) \leq \frac{\eta}{3}. \quad (80)$$

Hence, this leads to

$$|\hat{I}_{\text{ReNWJ}}(X, Y)_n - \hat{I}_{\text{ReNWJ}}(X, Y)| \leq \frac{\eta}{3} + \frac{\eta}{3} + \frac{\eta}{3} = \eta. \quad (81)$$

□

Theorem. *The ReNWJ estimator is strongly consistent.*

Proof. Let $\epsilon > 0$. We apply Lemma 12 and Lemma 13 to find a neural network function T_θ and $N \in \mathbb{N}$ such that Eq. (65) and Eq. (76) hold with $\eta = \epsilon/2$. By the triangular inequality, for all $n \geq N$ and with probability one, we have

$$\begin{aligned} |I(X, Y) - \hat{I}_{\text{ReNWJ}}(X, Y)_n| &= |I_{\text{ReNWJ}}(X, Y) - \hat{I}_{\text{ReNWJ}}(X, Y)_n| \quad (\because \text{ReNWJ representation}) \\ &\leq |I_{\text{ReNWJ}}(X, Y) - \hat{I}_{\text{ReNWJ}}(X, Y)| + |\hat{I}_{\text{ReNWJ}}(X, Y)_n - \hat{I}_{\text{ReNWJ}}(X, Y)| \leq \epsilon \end{aligned} \quad (82)$$

which proves the consistency. □

Sample complexity proof

Theorem. *Assume that the function $1 \leq |T_\theta| < M$ is \mathcal{L} -lipschitz with respect to the parameter θ . The domain θ is bounded, so that $\|\theta\| \leq K$ for some constant K . When using k mini-batches to estimate MI and $d(x, 1) \leq |x - 1|$, we have*

$$\mathcal{P}(|\hat{I}_{\text{ReNWJ}}(X, Y) - I(X, Y)| \leq \epsilon) \geq 1 - \delta \quad (83)$$

whenever the number of samples n for each batch satisfies

$$n \geq \frac{2M^2(d \log(24KL\sqrt{d}/\epsilon) + 2dM + \log(2/\delta))}{\epsilon^2 k}. \quad (84)$$

Proof. By taking the assumptions of Lemma 13, we begin with Eq. (78), Eq. (79) and Eq. (80). By the Hoeffding inequality, for all function f ,

$$\mathcal{P}(|\mathbb{E}_{\mathbb{Q}}[f] - \mathbb{E}_{\hat{\mathbb{Q}}}[f]| > \epsilon/6) \leq 2 \exp\left(-\frac{\epsilon^2(n \cdot k)}{2M^2}\right). \quad (85)$$

To extend this inequality to a uniform inequality over all functions T_θ and e^{T_θ} , we choose a minimal cover of the domain $\Theta \subset \mathbb{R}^d$ by a finite set of small balls of radius η , $\Theta \subset \cup_j B_\eta(\theta_j)$, and the union bound. The minimal cardinality of such covering is bounded by the covering number $N_\eta(\Theta)$ of Θ ,

$$N_\eta(\Theta) \leq \left(\frac{2K\sqrt{d}}{\eta}\right)^d. \quad (86)$$

Successively applying a union bound in Eq. (85) with the set of functions $\{T_{\theta_j}\}_j$, and $\{e^{T_{\theta_j}}\}_j$, We have

$$\mathcal{P}\left(\max_j |\mathbb{E}_{\mathbb{Q}}(T_{\theta_j}) - \mathbb{E}_{\hat{\mathbb{Q}}}(T_{\theta_j})| \geq \frac{\epsilon}{6}\right) \leq 2N_\eta(\Theta) \exp\left(-\frac{\epsilon^2(n \cdot k)}{2M^2}\right), \quad (87)$$

$$\mathcal{P}\left(\max_j |\mathbb{E}_{\mathbb{Q}}(e^{T_{\theta_j}}) - \mathbb{E}_{\hat{\mathbb{Q}}}(e^{T_{\theta_j}})| \geq \frac{\epsilon}{6}\right) \leq 2N_\eta(\Theta) \exp\left(-\frac{\epsilon^2(n \cdot k)}{2M^2}\right). \quad (88)$$

We now choose that ball radius to be $\eta = \frac{\epsilon}{12L}e^{-2M}$. Solving for n the inequation,

$$2N_\eta(\Theta) \exp\left(-\frac{\epsilon^2 n}{2M^2}\right) \leq \delta, \quad (89)$$

we deduce from Eq. (87) that, whenever Eq. (84) holds, with probability at least $1 - \delta$, for all $\theta \in \Theta$,

$$\begin{aligned} |\mathbb{E}_{\mathbb{Q}}(T_\theta) - \mathbb{E}_{\hat{\mathbb{Q}}}(T_\theta)| &\leq |\mathbb{E}_{\mathbb{Q}}(T_\theta) - \mathbb{E}_{\mathbb{Q}}(T_{\theta_j})| + |\mathbb{E}_{\mathbb{Q}}(T_{\theta_j}) - \mathbb{E}_{\hat{\mathbb{Q}}}(T_{\theta_j})| + |\mathbb{E}_{\hat{\mathbb{Q}}}(T_{\theta_j}) - \mathbb{E}_{\hat{\mathbb{Q}}}(T_\theta)| \\ &\leq \frac{\epsilon}{12}e^{-2M} + \frac{\epsilon}{6} + \frac{\epsilon}{12}e^{-2M} < \frac{\epsilon}{3}. \end{aligned} \quad (90)$$

Similarly, using Eq. (88), we get that with probability at least $1 - \delta$,

$$|\mathbb{E}_{\mathbb{Q}}(e^{T_{\theta-1}}) - \mathbb{E}_{\hat{\mathbb{Q}}}(e^{T_{\theta-1}})| \leq \frac{\epsilon}{3} < e \cdot \frac{\epsilon}{3}. \quad (91)$$

Hence,

$$\begin{aligned} |\hat{I}_{\text{ReNWJ}}(X, Y) - I(X, Y)| &\leq |\mathbb{E}_{\mathbb{Q}}(T_{\theta_j}) - \mathbb{E}_{\hat{\mathbb{Q}}}(T_{\theta_j})| + |\mathbb{E}_{\mathbb{Q}}(e^{T_{\theta_j-1}}) - \mathbb{E}_{\hat{\mathbb{Q}}}(e^{T_{\theta_j-1}})| + d(\mathbb{E}_{\mathbb{Q}}(e^{T_{\theta_j}}), \mathbb{E}_{\hat{\mathbb{Q}}}(e^{T_{\theta_j}})) \\ &\leq |\mathbb{E}_{\mathbb{Q}}(T_{\theta_j}) - \mathbb{E}_{\hat{\mathbb{Q}}}(T_{\theta_j})| + e^{-1}|\mathbb{E}_{\mathbb{Q}}(e^{T_{\theta_j}}) - \mathbb{E}_{\hat{\mathbb{Q}}}(e^{T_{\theta_j}})| + |\mathbb{E}_{\mathbb{Q}}(e^{T_{\theta_j}}) - \mathbb{E}_{\hat{\mathbb{Q}}}(e^{T_{\theta_j}})| \leq \epsilon. \end{aligned} \quad (92)$$

□

A.5 THE PROPERTY OF MI ESTIMATORS

The variance of the exponential value of the statistic network's output according to the bias of optimal functions on the distribution \mathbb{Q} .

Theorem. Let $Q^{(n)}$ be the empirical distributions of n i.i.d. samples from \mathbb{Q} . For the optimal $T_1 = \log \frac{dp}{dq} + C_1$ and $T_2 = \log \frac{dq}{dp} + C_2$ where $C_1 \geq C_2$,

$$\text{Var}_{\mathbb{Q}}(\mathbb{E}_{Q^{(n)}}(e^{T_1})) \geq \text{Var}_{\mathbb{Q}}(\mathbb{E}_{Q^{(n)}}(e^{T_2})). \quad (93)$$

Proof. Consider that

$$\text{Var}_{\mathbb{Q}}(e^{T_1}) = e^{2C_1} \left(\mathbb{E}_{\mathbb{Q}} \left(\left(\frac{d\mathbb{P}}{d\mathbb{Q}} \right)^2 \right) - \left(\mathbb{E}_{\mathbb{Q}} \left(\frac{d\mathbb{P}}{d\mathbb{Q}} \right) \right)^2 \right), \quad (94)$$

and

$$\text{Var}_{\mathbb{Q}}(e^{T_2}) = e^{2C_2} \left(\mathbb{E}_{\mathbb{Q}} \left(\left(\frac{d\mathbb{P}}{d\mathbb{Q}} \right)^2 \right) - \left(\mathbb{E}_{\mathbb{Q}} \left(\frac{d\mathbb{P}}{d\mathbb{Q}} \right) \right)^2 \right). \quad (95)$$

By Song and Ermon [2020], the variance of the mean of n i.i.d. random variable then gives us

$$\text{Var}_{\mathbb{Q}}(\mathbb{E}_{\mathbb{Q}^{(n)}}(e^{T_1})) = \frac{\text{Var}_{\mathbb{Q}}(e^{T_1})}{n}, \quad \text{Var}_{\mathbb{Q}}(\mathbb{E}_{\mathbb{Q}^{(n)}}(e^{T_2})) = \frac{\text{Var}_{\mathbb{Q}}(e^{T_2})}{n}. \quad (96)$$

Since $e^x \geq 1$ for all $x \geq 0$,

$$\frac{\text{Var}_{\mathbb{Q}}(\mathbb{E}_{\mathbb{Q}^{(n)}}(e^{T_1}))}{\text{Var}_{\mathbb{Q}}(\mathbb{E}_{\mathbb{Q}^{(n)}}(e^{T_2}))} = \frac{\frac{\text{Var}_{\mathbb{Q}}(e^{T_1})}{n}}{\frac{\text{Var}_{\mathbb{Q}}(e^{T_2})}{n}} = e^{2(C_1 - C_2)} \geq 1. \quad (97)$$

Therefore, the variance of T_1 is equal to or less than the that of T_2 on \mathbb{Q} . \square

Proof of estimation bias caused by drifting

Theorem. *When used on DV representation, the two averaging strategies below produce a biased MI estimate if the drifting problem occurs.*

1. *Macro-averaging (similar to that of Poole et al. [2019]): Establish a single estimate through the average of estimated MI from each batch.*
2. *Micro-averaging: Calculate the DV representation using the average of the each individual network outputs.*

Proof. We start from the definition of I_{DV} , where

$$I_{\text{DV}}(X, Y) = \mathbb{E}_{\mathbb{P}}(T(x, y)) - \log(\mathbb{E}_{\mathbb{Q}}(e^{T(x, y)})) \quad (98)$$

becomes the objective function to estimate MI, i.e. MINE.

Let $T_{ij}^{(J)}$ and $T_{ij}^{(M)}$ denote the ij -th element of outputs for \mathbb{P}_m and \mathbb{Q}_n respectively, where i is the index of batch and j is the index of sample inside the batch, and the non-drifting output as T_{ij}^* , and the drifting constant for each batch C_i . Then, $T_{ij} = T_{ij}^* + C_i$.

When the number of batch is B and each batch size is N ,

1. **Macro averaging:**

$$\frac{1}{B} \sum_i \left[\frac{1}{N} \sum_j T_{ij}^{(J)} - \log \left(\frac{1}{N} \sum_j e^{T_{ij}^{(M)}} \right) \right] \quad (99)$$

$$= \frac{1}{B} \sum_i \left[\frac{1}{N} \sum_j (T_{ij}^{(J^*)} + C_i) - \log \left(\frac{1}{N} \sum_j e^{T_{ij}^{(M^*)} + C_i} \right) \right] \quad (100)$$

$$= \frac{1}{B} \sum_i \left[\frac{1}{N} \sum_j (T_{ij}^{(J^*)} + C_i) - \log \left(\frac{1}{N} e^{C_i} \sum_j e^{T_{ij}^{(M^*)}} \right) \right] \quad (101)$$

$$= \frac{1}{B} \sum_i \left[\frac{1}{N} \sum_j T_{ij}^{(J^*)} - \log \left(e^{-C_i} \frac{1}{N} e^{C_i} \sum_j e^{T_{ij}^{(M^*)}} \right) \right] \quad (102)$$

$$= \frac{1}{B} \sum_i \left[\frac{1}{N} \sum_j T_{ij}^{(J^*)} - \log \left(\frac{1}{N} \sum_j e^{T_{ij}^{(M^*)}} \right) \right] \quad (103)$$

$$= \frac{1}{NB} \sum_{ij} T_{ij}^{(J^*)} - \frac{1}{B} \sum_i \left[\log \left(\frac{1}{N} \sum_j e^{T_{ij}^{(M^*)}} \right) \right] \quad (104)$$

$$\neq \frac{1}{NB} \sum_{ij} T_{ij}^{(J^*)} - \log \left(\frac{1}{NB} \sum_{ij} e^{T_{ij}^{(M^*)}} \right) \quad (105)$$

2. Micro averaging:

$$\frac{1}{NB} \sum_{ij} T_{ij}^{(J)} - \log\left(\frac{1}{NB} \sum_{ij} e^{T_{ij}^{(M)}}\right) \quad (106)$$

$$= \frac{1}{NB} \sum_{ij} (T_{ij}^{(J^*)} + C_i) - \log\left(\frac{1}{NB} \sum_{ij} e^{(T_{ij}^{(M^*)} + C_i)}\right) \quad (107)$$

$$= \frac{1}{NB} \sum_{ij} T_{ij}^{(J^*)} - \log\left[\left(\frac{1}{NB} \sum_{ij} e^{(T_{ij}^{(M^*)} + C_i)}\right)^{\frac{1}{B} \sum_i C_i}\right] \quad (108)$$

$$\neq \frac{1}{NB} \sum_{ij} T_{ij}^{(J^*)} - \log\left(\frac{1}{NB} \sum_{ij} e^{T_{ij}^{(M^*)}}\right) \quad (109)$$

□

We emphasize that we have to stop the drifting via the regularization term of ReDV.

Wrong estimation derived from biased values According to the theorem above, the MI estimate derived from the average of the values estimated from the mini-batch in DV representation-based estimators will lead to erroneous results. However, the micro-averaging strategy is often used to measure the performance of MI estimators (MINE or InfoNCE), as shown in Fig. 6 of Cheng et al. [2020].

A.6 THE PROOF FOR THE VALIDITY OF OUR BENCHMARK

We assume that the dataset used for our benchmark satisfies the single label assumption where there exists exactly one label for every sample inside the dataset. Note that the assumption implies that $p(y|x) = 1$. In other words, we assume statistical dependence between X and Y [Tishby and Zaslavsky, 2015].

Theorem. (*Supervised Learning Benchmark*) Consider a dataset $D = (X, Y)$ where Y is the label for sample X , and $H(Y)$ is the entropy of Y .

$$I(X, Y) = H(Y) \quad (110)$$

Proof.

$$I(X; Y) = \int_{X, Y} P(X, Y) \log \frac{P(X, Y)}{P(X)P(Y)} \quad (111)$$

$$= \int_x \int_y P(x, y) \log \frac{P(y|x)}{P(y)} dy dx \quad (112)$$

$$= \int_x \int_y P(x) P(y|x) \log \frac{P(y|x)}{P(y)} dy dx \quad (113)$$

$$= \int_x P(x) \left(\int_y P(y|x) \log \frac{P(y|x)}{P(y)} dy \right) dx \quad (114)$$

$$= \int_R P(x^*) \log \frac{1}{P(y^*)} \quad (\text{where } R \text{ is the region where } y^* \text{ is a correct label for the given } x^*) \quad (115)$$

$$= \sum_c \int_{R_c} P(x^*, c) \log \frac{1}{P(c)} \quad (\text{where } R \text{ is partitioned by the label } c \text{ to yield } R_c) \quad (116)$$

$$= \sum_c \log \frac{1}{P(c)} \int_{R_c} P(x^*, c) \quad (\because P(c) \text{ is constant inside the } R_c) \quad (117)$$

$$= \sum_c \log \frac{1}{P(c)} P(c) \quad (\because \int_{R_c} P(x^*, c) = P(c), \text{ i.e., marginalization}) \quad (118)$$

$$= H(Y) \quad (119)$$

□

Theorem. (Contrastive Learning Benchmark) Consider a dataset $D = (X, Y)$. Let X_1 be a sample drawn from the dataset with the label Y and X_2 be another sample drawn from the subset of D where all the samples inside the subset are with the same label Y . Assume that D also satisfies the single label assumption.

$$I(X_1, X_2) = I(X_1, Y) = I(X_2, Y) = H(Y) \quad (120)$$

Proof.

$$\begin{aligned} P(X_1, X_2) &= \sum_{y_i} P(X_1, X_2, Y) \quad (\because \text{marginalization}) \\ &= \sum_{y_i} P(X_1)P(Y|X_1)P(X_2|Y, X_1) \quad (\because \text{factorization}) \\ &= \sum_{y_i} P(Y)P(X_1|Y)P(X_2|Y) \quad (\because X_1 \text{ and } X_2 \text{ are independent for given } Y) \\ &= \sum_i P(y_i)P(X_1|y_i)P(X_2|y_i) \end{aligned}$$

$$\begin{aligned} P(X_1) &= \sum_{y_i} P(X_1, Y) = \sum_{y_i} P(Y)P(X_1|Y) = \sum_i P(y_i)P(X_1|y_i) \\ P(X_2) &= \sum_{y_i} P(X_2, Y) = \sum_{y_i} P(Y)P(X_2|Y) = \sum_i P(y_i)P(X_2|y_i) \end{aligned}$$

$$\begin{aligned} \frac{P(X_1, X_2)}{P(X_1)P(X_2)} &= \frac{\sum_i P(y_i)P(X_1|y_i)P(X_2|y_i)}{\sum_i P(y_i)P(X_1|y_i) \sum_{y_i} P(y_i)P(X_2|y_i)} \\ &= \frac{\sum_i P(y_i)P(X_1|y_i)P(X_2|y_i)}{\sum_i P(y_i)^2 P(X_1|y_i)P(X_2|y_i)} \quad (\because X_1 \text{ and } X_2 \text{ has the same label}) \end{aligned}$$

Let R_i be the region where (X, y_i) such as i -th class label y_i is a correct label for the given X_1 .

$$\begin{aligned} I(X_1, X_2) &= \int_{X_1, X_2} P(X_1, X_2) \log \frac{P(X_1, X_2)}{P(X_1)P(X_2)} \\ &= \int_{X_1, X_2} \left(\sum_i P(y_i)P(X_1|y_i)P(X_2|y_i) \right) \log \frac{\sum_i P(y_i)P(X_1|y_i)P(X_2|y_i)}{\sum_i P(y_i)^2 P(X_1|y_i)P(X_2|y_i)} \\ &= \sum_i P(y_i) \int_{X_2} P(X_2|y_i) \left(\int_{R_i} P(X_1|y_i) \log \frac{P(y_i)P(X_1|y_i)P(X_2|y_i)}{P(y_i)^2 P(X_1|y_i)P(X_2|y_i)} dx_1 \right) dx_2 \\ &= \sum_i P(y_i) \int_{X_2} P(X_2|y_i) \left(\int_{R_i} P(X_1|y_i) \log \frac{1}{P(y_i)} dx_1 \right) dx_2 \\ &= \sum_i P(y_i) \log \frac{1}{P(y_i)} \int_{X_2} P(X_2|y_i) \left(\int_{R_i} P(X_1|y_i) dx_1 \right) dx_2 \\ &= \sum_i P(y_i) \log \frac{1}{P(y_i)} \\ &= H(Y) \end{aligned}$$

□

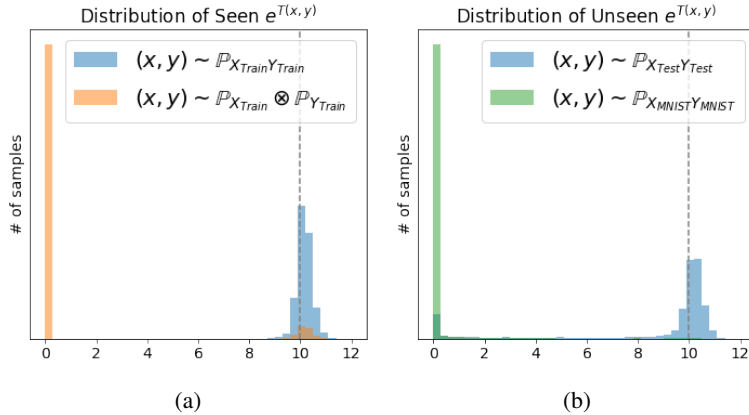


Figure 8: Histogram of the exponential of the network outputs $e^{T(x,y)}$ which is trained with CLB CIFAR10. Training samples and unseen samples are fed to (a) and (b), respectively.

B DIRECTLY UTILIZING THE STATISTICS NETWORK OUTPUTS FOR OUT-OF-DISTRIBUTION TASK

We observe the SLB CIFAR10-trained network outputs when seen or unseen samples are fed to the statistics network T in Fig. 8. Note that we can take $e^{T(x,y)} = \frac{d\mathbb{P}_{XY}}{d\mathbb{P}_X \otimes \mathbb{P}_Y}$ for granted, thanks to regularization. Fig. 8 (a) shows the distribution of $e^{T(x,y)}$ for the training set samples $(x,y) \sim \mathbb{P}_{X_{\text{Train}}Y_{\text{Train}}}$. As 90% of $(x,y) \sim \mathbb{P}_X \otimes \mathbb{P}_Y$ is wrongly labeled, the majority yields $e^{T(x,y)} = 0$. The likelihood ratio for the $(x,y) \sim \mathbb{P}_{XY}$ is 10, and all the samples are centered around the ideal value as expected. CIFAR10 test set samples $(x,y) \sim \mathbb{P}_{X_{\text{Test}}Y_{\text{Test}}}$ also yield similar results, where some of the samples are wrongly positioned, being the test error of T . Surprisingly, when we feed MNIST [LeCun et al., 1998] training samples $(x,y) \sim \mathbb{P}_{X_{\text{MNIST}}Y_{\text{MNIST}}}$, model successfully classifies nearly all the samples to be less likely to occur in $\mathbb{P}_{X_{\text{Train}}Y_{\text{Train}}}$. This implies that exploiting the network outputs with the viewpoints of MI may show usefulness in out-of-distribution detection.

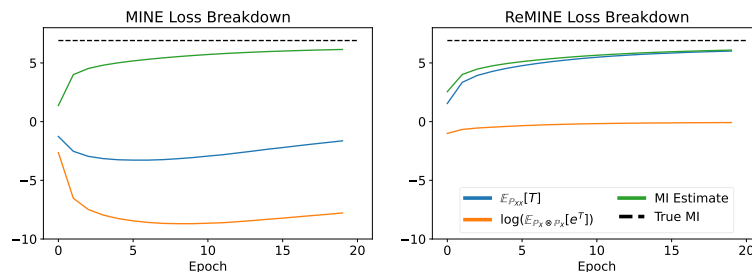


Figure 9: Training T_θ using I_{MINE} and I_{ReMINE} with batch size 100 for 20 epochs. We breakdown the MI loss into two components. We split both losses into first term $\mathbb{E}_{\mathbb{P}_{XX}}(T)$ and second term $\log \mathbb{E}_{\mathbb{P}_X \otimes \mathbb{P}_X}(e^T)$.

C EXPERIMENTS ON IMAGENET

We test on the ImageNet dataset with 1000 classes, where we use the batch size of 100. We set the batch size to be relatively small to observe how different losses behave, whereas multiple contrastive learning literature such as Chen et al. [2020], He et al. [2020] uses large batch sizes to avoid instability. We train for 20 epochs to observe the early stages of training.

First, we can observe in Fig. 9 that the regularizer successfully solves the drifting problem of I_{MINE} . Also, Table 3 shows that I_{NWJ} fails in the contrastive learning benchmark. I_{NWJ} explodes within a few steps of training, where the regularizer successfully avoids the problem to yield a feasible output. Note that we did not observe the losses till convergence; we have to train much longer to obtain a more accurate performance of MI estimation and test accuracy. However, we can see

Task	Loss	MI Estimation		Test Accuracy	
		Original	Regularized	Original	Regularized
Supervised Learning Benchmark	CE	-	-	0.0795	-
	MINE	6.147	6.110	0.1056	0.1081
	NWJ	6.072	6.075	0.1020	0.1005
Contrastive Learning Benchmark	MINE	1.095	1.140	0.0103	0.0098
	NWJ	0.000	1.008	0.0010	0.0072

Table 3: Our supervised and contrastive learning benchmark results on ImageNet dataset. We provide the MI estimation and test accuracy, where we clip the negative MI estimations to 0. We compare the performance of original and regularized loss. We also add the accuracy of standard cross-entropy loss (CE) for comparison. Similar to Section 5.2, we choose the regularization weight $\lambda \in \{0.1, 0.01, 0.001\}$ that shows the best MI estimation results.

that in the supervised learning benchmark, which is the relatively easier benchmark, all the losses are already close to the optimal MI even in the earlier epochs. We can also observe a similar trade-off between the MI estimation and test accuracy in Table 3. Future works on large-scale datasets are needed to observe the behaviors further.

D EXPERIMENTAL DETAILS

In this section, we provide the experiment details in the manuscript with the accompanying code <https://github.com/Siyeong-Lee/Deconstructing-MINE>.

D.1 HARDWARE SPECIFICATION

We use a single NVIDIA DGX A100 machine with 8 GPUs for all the experiments. All the experiments except for our benchmark experiments take less than 10 minutes and a single GPU to compute. It takes less than 2 days to compute all the benchmark experiments: 4 settings, 12 losses, and 5 seeds running on 8 GPUs and 4 processes per GPU.

D.2 DETAILED SETTINGS FOR ONE-HOT DATASET EXPERIMENTS

We describe the detailed settings for Fig. 1, Fig. 2, Fig. 3, Fig. 4, and Fig. 5. We choose $N = 16$ for the one-hot discrete dataset $X \sim U(1, N)$. We use a simple statistics network T with a concatenated vector of dimension $N \times 2 = 32$ as input. We pass the input through two fully connected layers with ReLU activation by widths: $32 - 256 - 1$. The last layer outputs a single scalar with no bias and activation. We use stochastic gradient descent (SGD) with learning rate 0.1 to optimize the statistics network unless specified.

D.3 DETAILED SETTINGS FOR OUR BENCHMARK

We describe the detailed settings for Table 2 and Fig. 6. We use ResNet-18 [He et al., 2016] as the backbone network and use Adam optimizer with the default learning rate 0.001, $\beta_1 = 0.9$ and $\beta_2 = 0.999$. We use batch size 100 for CIFAR100 and 10 for CIFAR10. We train for different epochs per each benchmark: 40 epochs (SLB CIFAR10), 100 epochs (SLB CIFAR100), 100 epochs (CLB CIFAR10), and 150 epochs (CLB CIFAR100). We choose enough number of epochs for all the losses to be fully converged for each of the benchmarks. We rerun the same experiment 5 times with different seeds.

D.4 DETAILED SETTINGS FOR THE 20D CORRELATED GAUSSIAN TASK

We describe the detailed settings for Fig. 7. We sampled (x, y) from d -dimensional correlated Gaussian dataset where $X \sim N(\mathbf{0}, \mathbf{I}_d)$ and $Y \sim N(\rho X, (1 - \rho^2)\mathbf{I}_d)$ given the correlation parameter $0 \leq \rho < 1$, which is taken from Belghazi et al. [2018]. The true MI for the dataset is $I(X, Y) = -\frac{d}{2} \log(1 - \rho^2)$. For the statistics network architecture, we consider the architecture similar to Appendix D.2 where we concatenate the inputs (x, y) to pass through three fully connected layers with ReLU activation (excluding the output layer) by widths $40 - 256 - 256 - 1$, same as the network used in Poole et al. [2019]. We used the same optimizer with Appendix D.3.